Manuscript submitted to **Biophysical***Journal*
Article

Biophysical Studies of Lipid Nanodomains using Different Physical Characterization Techniques

Jacob J. Kinnun[1,2], Haden L. Scott[1,2], Dima Bolmatov[2,3], C. Patrick Collier[4], Timothy R. Charlton[1], and John Katsaras[2,3,5]

[1]Large Scale Structures Group, Neutron Scattering Division, Oak Ridge National Laboratory, Oak Ridge, TN 37831, United States
[2]Shull Wollan Center, Oak Ridge National Laboratory, Oak Ridge, Tennessee 37831, United States
[3]Department of Physics and Astronomy, University of Tennessee, Knoxville, TN 37996, United States
[4]Center for Nanophase Materials Sciences, Oak Ridge National Laboratory, Oak Ridge, Tennessee 37831, United States
[5]Labs and Soft Matter Group, Neutron Scattering Division, Oak Ridge National Laboratory, Oak Ridge, TN 37831, United States
[*]Correspondence: kinnunjj@ornl.gov
[*]Correspondence: katsarasj@ornl.gov

ABSTRACT For the past 50 years, evidence for the existence of functional lipid domains has been steadily accumulating. Although the notion of functional lipid domains, also known as “lipid rafts”, is now widely accepted, this was not always the case. This ambiguity surrounding lipid domains could be partly attributed to the fact that they are highly dynamic, nanoscopic structures. Since most commonly used techniques are sensitive to microscale structural features, it is therefore not surprising that it took some time to reach a consensus regarding their existence. In this review article we will discuss studies which have used techniques that are inherently sensitive to nanoscopic structural features (i.e., neutron scatting, nuclear magnetic resonance, and Förster resonance energy transfer). We will also mention techniques that may be of use in the future (i.e., cryo-EM, droplet interface bilayers, inelastic X-ray scattering, and neutron reflectometry), which can further our understanding of the different and unique physicochemical properties of nanoscopic lipid domains.

SIGNIFICANCE Membrane nandomains, including lipid rafts, in biological membranes have been a hot topic in research over the past few decades. Once controversial, lipid rafts now are believed to be nanoscopic, transient, and highly dynamic structures. Due to their small and dynamic nature, many techniques have had difficulty studying these nanodomains. Here we report on established (neutron scatting, nuclear magnetic resonance, and Förster resonance energy transfer) and emerging techniques (cryo-EM, droplet interface bilayers, inelastic X-ray scattering, and neutron reflectometry) which have molecular-scale sensitivities, and describe how these techniques have been used to measure fundamental properties of lipid nanodomains (i.e. size, composition, and molecular structure).

1 INTRODUCTION

The lipid bilayer is now accepted as being the underlying structure of cell membranes. However, this was not always the case. In the late 1800s, Charles Overton conducted a series of experiments that demonstrated the boundary layer surrounding cells contained lipids (1). However, it was not until 1925 that Gorter and Grendel, using red blood cells and a Langmuir trough – developed by Agnes Pockels (2) and refined by Irving Langmuir (3) – who presented convincing evidence that the lipid bilayer was indeed the underlying structure of biological membranes(4).

Although the discovery by Gorter and Grendel advanced our understanding of the boundary layer surrounding cells, the existence of a simple lipid bilayer could not explain many of the physicochemical properties associated with it. To address its electrical and permeability properties, Danielli and Davson (1935) proposed a model made up of a thin “lipoid film”, onto which proteins were adsorbed, resulting in a protein-lipid-protein “sandwich” structure (5), as shown in Fig. 1A. This model could, in theory, explain the differential sensitivity of the cell surface to molecules of different sizes and solubilities, as well as ions of different charge. More importantly, however, the Danielli-Davson model of the cell membrane highlighted the significance of proteins in biological membranes.

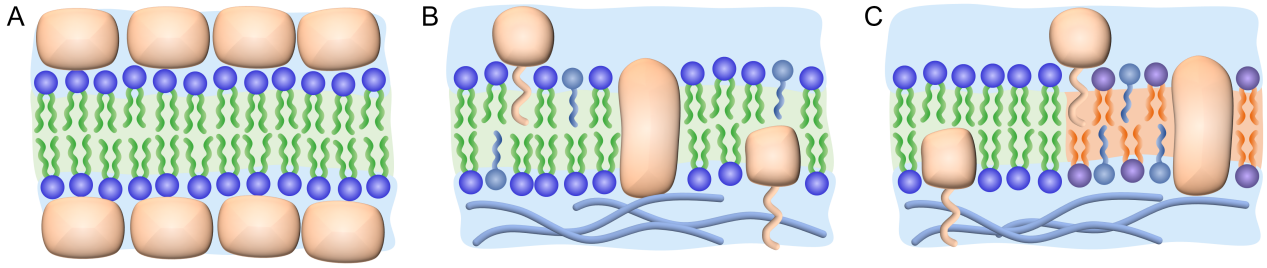

Figure 1: Cartoon of membrane evolution. As models for biological membranes have evolved, they have yielded a more detailed picture of the plasma membrane (PM). (A) The evolution of the 1920s Gorter and Grendel membrane (1, 4) by Danielli and Davson, where the lipid bilayer was sandwiched between adsorbed protein films (5) in order to address some of the PM's physicochemical properties. Protein-inclusive models advanced to include cytoskeletal elements and biomolecular diversity, culminating in the fluid mosaic model by Singer and Nicholson(6). Although evidence for lipid domains existed when the fluid mosaic model of the PM was proposed (e.g., (7–10), it was not until the late 1990s, when Simons and Ikonen proposed the lipid raft model (C) (11) that researchers started to carry out systematic studies to characterize them *in vivo*

.

In 1931, Max Knoll and Ernst Ruska (12) developed a prototype electron microscope (EM) with 400 power magnification. A couple of years later, von Borries and Ruska built the first EM which exceeded the resolution of an optical microscope (13). The development of the EM allowed for more detailed studies of the cell PM, and it was this capability that J. David Robertson used to eventually develop his unit membrane model (14). Specifically, using fixing agents, such as osmium tetroxide and potassium permanganate, Robertson and co-workers observed cell membranes from nerve fibers and other tissues, as triple-layered structures consisting of two dense layers, bordering a light central zone of approximately equal thicknesses. Although Robertson's unit membrane model was not unlike the one proposed by Danielli and Davson (5), it nevertheless highlighted two enduring features: (i) that the lipid bilayer is the underlying structure of all membranes; and (ii) that biological membranes are chemically asymmetric.

The main drawbacks of the unit membrane model was that it did not address the dynamic nature of cell membranes and the proteins did not penetrate the lipid bilayer – i.e., they only associated with the bilayer surface. In 1972, Singer and Nicolson proposed the now well known fluid mosaic model (Fig. 1B) of the PM, which addressed the two above-mentioned deficiencies of Robertson's unit membrane model (6). Namely, in addition to the peripheral proteins which were held to the membrane by electrostatic and weak noncovalent interactions, there were proteins which embedded themselves into the fluid bilayer. These so-called integral membrane proteins interacted with the membrane to a higher degree and although they are randomly distributed over large length scales, they could form aggregates over short distances, with lipids interacting with specific proteins (6). The 1972 paper by Singer and Nicolson also implied the presence of lateral heterogeneity, but the idea that lateral heterogeneity was somehow related to biological function was still to come (15).

The notion of lipid domains was hypothesized shortly after the publication of the fluid mosaic model of the PM (7–9). Moreover, in the 1980s it became known that PM domains possessed unique lipid and protein compositions (10) and that sphingomyelin and glucosylceramide were sorted into domains by the cell's machinery (16). In 1997, Simons and Ikonen (11) proposed the now well-known, but at the time, controversial "lipid raft" theory that stated that sphingolipids and cholesterol dynamically form domains (Fig. 1C), which act as platforms for protein-lipid interactions and as relay stations for intracellular signaling. However, the theory was brought into question as it was based on data that biological membranes exhibit resistance to solubilization by detergents such as, Triton X-100. (It should be noted that Triton X-100 can potentially promote domain formation in homogeneous lipid mixtures – although evidence has varied – which argues against the idea that detergent-resistant membranes are a hallmark of functional rafts.)(17–19) Further a controversy remains on the correlation between rafts and biological function.(20) Finally, in light of there being no "direct" evidence for lipid rafts from optical microscopy studies, it was suggested that rafts were perhaps, dynamical, nanoscopic supramolecular structures (21, 22).

In this review article we will describe recent studies reporting on the static and dynamic structures of nanoscopic lipid domains in both model and *in vivo* membrane platforms. Since lipid domains have been debated from when they were first proposed, researchers have used a range of experimental techniques to study them. Here, we will primarily focus on techniques that are inherently sensitive to nanoscopic structures and often short time scales, as much of the current research points to lipid domains being nanoscopic in size and transient in nature.(23, 24) Importantly, we will also highlight new and interesting physical techniques that may potentially help us to further understand the physical nature of lipid domains.

2 FUNDAMENTAL TECHNIQUES

Neutron scattering, NMR, and Förster resonance energy transfer (FRET) are established techniques used to detect nanometer-scale lateral heterogeneities in membranes. Neutron scattering and NMR are sensitive to nuclear properties – spatial density for neutron scattering and magnetic moment for NMR – which enables them to interrogate nanoscale features through isotopic labeling (e.g., substitution of protium for deuterium). With FRET, acceptor and donor fluorophores are used to transfer energy transfer, enabling the technique to detect small changes in distance. Thus neutron scattering, NMR, and FRET have been used extensively to study the lateral structure of phase separated membranes.

2.1 Neutron Scattering

The neutron was discovered by James Chadwick in 1932. (25) It was then quickly realized that this new uncharged particle could be used to probe atomic nuclei. In contrast to x-rays, neutrons scatter from atomic nuclei and do so, in a somewhat random fashion, by different elements throughout the periodic table. For example, the coherent scattering length, or the ability to scatter neutrons, is practically the same for hydrogen and aluminum – not so for x-rays – even though they differ greatly in atomic number. More importantly for the current discussion, is that the different hydrogen isotopes (i.e., protium, deuterium and tritium) also scatter very differently from each other(26). This unique property of neutrons enables the powerful neutron scattering protocol known as contrast variation which allows one to systematically highlight, or attenuate, different features of a complex system (27–32). In some cases, such as viruses that are primarily made up of a nucleic acid core surrounded by a protective protein coating, the thickness of the core and coating – because they differ in their scattering abilities – can be determined simply by changing the H_2O/D_2O ratio of the solvent, such that only one of the two structural features (nucleic acids or protein) is "visible" to neutrons (33–35). Moreover, through the use of deuterated biomolecules, one can methodically alter and create neutron contrast to detect the presence of nanoscopic lipid domains.

2.1.1 Small Angle Neutron Scattering

The wavelength of neutrons is on the order of Ångstroms, as such, they are capable of detecting nanoscopic membrane features. However, to do so, one needs to introduce neutron contrast such that the lipid domains differ in scattering ability from their surrounding environment. This can be accomplished, for example, through the selective deuteration of a lipid that preferentially partitions into one of the two lipid phases (i.e., the domain or its surround) (36, 37). The H_2O/D_2O solvent ratio is then adjusted such that, one of the two phases is contrast matched to the solvent, making only one phase "visible" to neutrons. From the resultant SANS data, and differential scanning calorimetry, one is then able to determine the size and composition of the lipid domains and the size of, for example, the spherical unilamellar vesicles (ULVs) that they populate (38–41). Using this approach, Pencer et al. (36) made use of small angle neutron scattering (SANS) and selective deuteration to observe lipid domains approximately 20 nm in diameter in 1:1:1 lipid mixtures of dioleoyl phosphatidylcholine (DOPC), chain-deuterated dipalmitoyl phosphatidylcholine (dDPPC), and cholesterol. Replacing DOPC with stearoyl oleoyl phosphatidycholine (SOPC) eliminated the lipid domains, highlighting the importance of lipid composition in domain formation and stability.

The Pencer et al. study (36) was extended by Heberle et al. (28) using the well-characterized, four component phase separating lipid mixture of distearoyl phosphatidycholine (DSPC), DOPC, palmitoyl oleoyl phosphatidycholine (POPC), and cholesterol (42, 43). In addition, Heberle and co-workers(28) used chain perdeuterated DSPC (DSPC-d_{70}) and 60 nm diameter ULVs to study the size of lipid domains and bilayer thickness mismatch between the domains and their surround, as a function of DOPC:POPC ratio (fig. 3). They not only found that domain size increased as a function of increasing amounts of the non-biologically relevant lipid, DOPC, but that bilayer thickness mismatch also increased with increasing domain size. In addition, the study by Heberle et al. experimentally demonstrated that line tension plays a dominant role in controlling domain size in free-floating bilayers (44). It should also be mentioned that with a few exceptions (45), scattering data is fitted using a real space model. Heberle et al. (28) fitted the different SANS profiles using a modified coarse-graining method, where the lipids in the ULVs were represented by uniformly-sized beads that were randomly placed using a pseudo-random generator (36).

Although much of the literature about functional lipid domains has focused on cholesterol-rich domains in mammalian membranes, there was mounting evidence that these structures were present in all biological membranes (46–48). Direct evidence for macroscopic lipid domains — using fluorescent dyes — was made by the visualization of cardiolipin domains in *E. coli* (49) and *Bacillus subtilis* (50), thus also confirming the existence of membrane heterogeneity in bacterial membranes, ergo their importance to physiological function. However, the *in vivo* measurement of lipid domain size remained elusive.

Compared to *in vitro* neutron studies, *in vivo* studies are much less common. This is a direct result that biological cells are made up of different classes of biomolecules (lipids, proteins, carbohydrates, etc.), each with its own unique scattering signature. Thus, it is impossible to isolate the scattering arising from only the PM in an intact cell. As a consequence, *in vivo* neutron studies have, to a great extent, relied on the use of basic neutron contrast variation schemes (51–54). A popular *in*

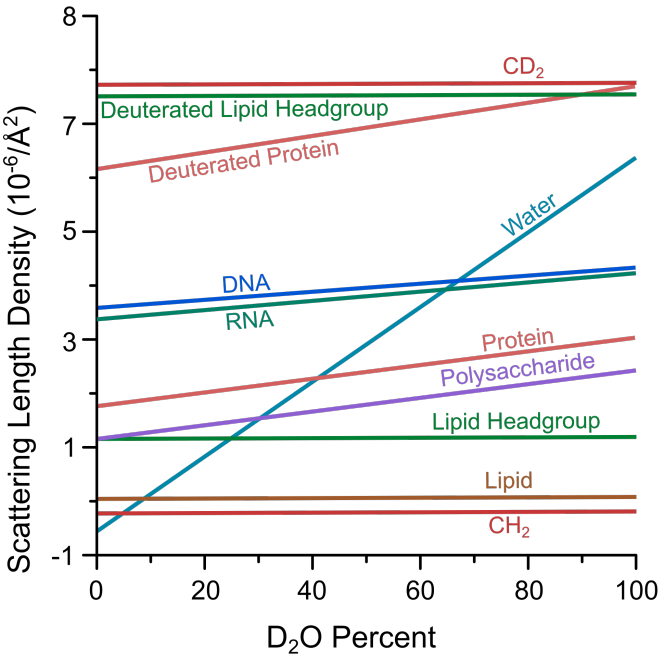

Figure 2: Neutron contrast variation. At given H_2O/D_2O ratios, different biomolecules (e.g., proteins, lipids, polysaccharides, DNA) can be made "invisible" to neutrons (i.e., when the water line intersects the line associated with a given class of biomolecules). For example, proteins and lipids have different match points, namely at 8% and 41% H_2O/D_2O ratios , respectively.

vivo system has been thylakoid membranes — due to its periodic organization, which gives rise to statistically meaningful and interpretable data (52–54). However, it was not until the 2017 Nickels et al. study that the full potential of neutron contrast variation was realized in an *in vivo* system, namely through the use of genetic and chemical manipulation of the Gram-positive bacterium, *Bacillus subtilis*, where the protium and deuterium content of the cell, and its membrane, were independently and systematically controlled (30).

Nickels and co-workers described a scheme where the chemistry, and thus the neutron contrast of the single-membrane bacterium, *B. subtilis*, was controlled through genetic and chemical manipulation. *B. subtilis* was chosen because it was: (i) genetically tractable; (ii) its lipid metabolism was well-characterized; (iii) it could be readily grown in deuterated media; and (iv) its single membrane is entirely made up of saturated fatty acids that could be deuterated, allowing for neutron contrast to be easily implemented and controlled. Growing the cells in deuterated media replaced almost all of the protiums with deuteriums throughout the cell, upon which neutron contrast was then reintroduced into the membrane by making protiated fatty acids readily available to the bacteria, which they incorporated in their PM membranes. Doing so allowed Nickels et al. (30) to measure the lipid bilayer thickness *in vivo*. Subsequently, by modifying the labeling scheme, they were able to make the first *in vivo* size measurement of nanoscopic lipid domains without using a molecular probe.

2.1.2 Neutron Spin Echo

Neutron spin echo (NSE) is an inelastic neutron scattering technique (55) that measures the relaxation rates of membrane fluctuations that are affected both by viscosity and the static bending modulus, κ. κ is an intensive property that describes the membrane's tendency to resist bending and it depends on membrane composition and temperature. Using the same lipid composition mixtures and vesicle sizes as those by Heberle et al. (28), Nickels et al. (29) combined NSE and molecular dynamics (MD) simulations to examine the bending moduli of lipid domains populating 60 nm diameter ULVs – note that MD simulations describe the movement of atoms and molecules, whose trajectories are numerically determined by solving Newton's equations of motion (56). Importantly, the combined use of NSE and MD provided a molecular picture of the membrane, which one could not have formulated from experiment alone.

Through selective deuteration, NSE and MD simulations, Nickels et al. (29) were able to determine the bending moduli of lipid domains and those of their surroundings. Unsurprisingly, they determined that κ of nanoscopic domains differs from the

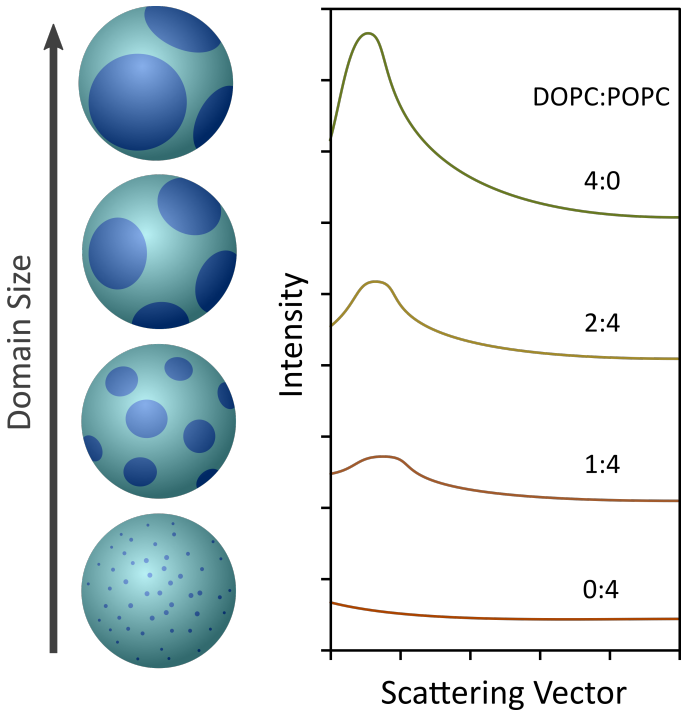

Figure 3: Schematic of changes in scattering as a function of domain size. Heberle et al. studied the four component phase separating lipid mixture of DSPC, DOPC, POPC, and cholesterol using SANS. Chain perdeuterated DSPC (DSPC-d_{70}) was used to introduce neutron contrast and the H_2O/D_2O solvent ratio was adjusted to match an ideally mixed lipid membrane, i.e., no lipid domains at an elevated temperature. The presence of a SANS signal (right) indicated the existence of lipid domains, which grew in intensity with increasing domain size due to an increasing DOPC:POPC ratio. Domain size was determined by fitting the SANS data using a modified coarse-graining method (28, 36).

continuous phase surrounding them. In conjunction with MD simulations, they were also able to determine that the lipids in nanoscopic domains were in registry across the bilayer leaflets. Fitting the NSE data using MD simulations produced a molecular description of the nanodomain interface with its surrounding phase. Of note, was that nanodomain interfaces were enriched in POPC and that multiple mechanisms were found to be responsible for producing stable nanoscopic lipid heterogeneities. Recently, Himbert et al. (57) using diffuse x-ray scattering, NSE, and MD simulations determined the κ of red blood cell (RBC) "ghosts". Typically literature values of the bending rigity of RBCs vary by orders of magnitude, however they studied the cytoplasmic membrane in the absence of spectrin and adenosine triphosphate to reduce potential variability. They found bending rigidities that were relatively small compared to literature values and of single component lipid bilayers. This smaller κ may contribute to reducing the energy costs of the process where RBCs have to continuously undergo shape changes as they navigate from larger diameter arteries/veins to small capillaries, and back.

2.2 Nuclear Magnetic Resonance

One hundred years ago, Stern and Gerlach demonstrated that the nuclear angular momentum in a magnetic field is quantized, a phenomenon explained by nuclear spin states (58). Later on, Isidor I. Rabi would improve on the measurements by Stern and Gerlach by using the absorption of radio-frequency radiation to observe the resonance of nuclei in a magnetic field. This gave rise to the technique we now know as NMR (59), earning Rabi the 1944 Nobel prize in physics. NMR's sensitivity was further increased through the use of the pulse-Fourier transform approach developed by Ernst(60). Specifically, the NMR signal observed from nuclear precession is Fourier transformed to produce a spectrum which can be readily analyzed. The precession is sensitive to the electromagnetic environment of the nucleus, which produces shifts (chemical shift) and line shape changes (anisotropy) to the NMR signal, as shown in Fig. 4A. In general, NMR is sensitive to the orientation of the sample with respect to the magnetic field. In liquids this orientational dependence is typically averaged due to the rapid reorientation of molecules. However, for large molecules, such as proteins and liquid crystals (e.g., membranes), reorientation is slow compared to the Larmor frequency of the nuclei and a broad line shape is observed. Since this is a measurement at the atomic scale, NMR is

sensitive to the presence of small structures in the membrane, including nanometer-sized domains.

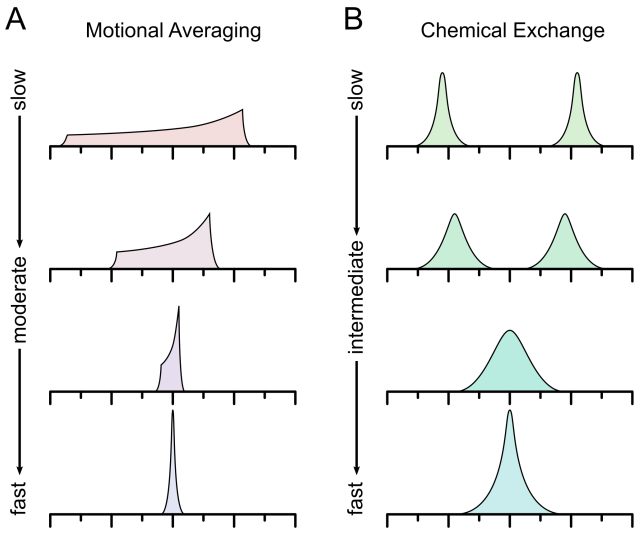

Figure 4: Motional averaging and chemical exchange. In NMR, the precession of the nuclei in a magnetic field is sensitive to their orientations and motions. (A) Orientational dependence of the interaction between nuclei and their environment typically results in a so-called "Pake" powder line shape. Rapid re-orientation of the nuclei causes the line shape to narrow. Since ^{2}H is a spin-one nucleus, there are two possible spin transitions, resulting in a symmetrized powder pattern. (B) Nuclei in different magnetic environments will produce distinct resonances in their spectra. If the nucleus is exchanging between the different environments, it experiences chemical exchange. At intermediate rates of exchange, the distinct resonance for each environment will begin to average and the line shapes will broaden. At faster rates of exchange, their resonances will merge into a single homogeneous resonance.

The presence of domains in the membrane alters the line shape of the NMR spectrum according to the rate of chemical exchange of lipids between domains, compared to the resonance frequency of the nucleus (see fig. 4B). If the rate of exchange is fast, a single homogeneous line shape will occur, and if the exchange is slow, then a superposition of line shapes will appear due to differences in domains — in the intermediate range one observes a broadened line shape. Whether the exchange rate appears to be slow, intermediate, or fast depends on three factors: (i) the resonance frequency of the nucleus in the magnetic field; (ii) the diffusion rate of the lipid; (iii) and the size of the domains. The rate of exchange (κ) for intermediate exchange is approximated by:

$$\kappa \approx \pi \left(\Delta\nu^o - \Delta\nu^d \right), \tag{1}$$

where ν^o is the line shape width of the ordered phase and ν^d is that of the disordered phase (61). If the exchange is fast, the exchange rate is greater than the value calculated from Eq. 1 and vice versa. If the exchange rate and the lipid rate of diffusion (D) are known, the average distance a lipid traveled to exchange with the adjacent domain (d) can be calculated as:

$$d = 4\sqrt{2\frac{D}{\kappa}}. \tag{2}$$

By assuming the shape of the domain, a domain size can be estimated (61). For liquid-liquid domains, a circular domain shape is a good first approximation. However, in the case of slow and fast exchange, only lower and upper limits, respectively, of domain size can be calculated. In which regime exchange occurs depends on how the rate of exchange relates to the NMR time scale. The NMR time scale is not a fixed and depends on the nucleus, method, and spectrometer. Chemical shift differences for ^{1}H NMR spectra can be in the Hz region (i.e., milliseconds), thus only very large domains can be discerned. However, for nuclei such as, ^{1}3C and ^{3}1P chemical shift differences are much larger and the time scales much smaller. In the case of of ^{2}H NMR, the anisotropic lineshape patterns can have spectral differences in the kHz range (microsecond time scale), allowing for the observation of nanometer sized domains in the slow exchange regime. As we will see, this does not rule out ^{1}H NMR as a technique to study nanometer sized domains, as lineshape broadening, due to relaxation, is sensitive to short time scales (microseconds to nanoseconds) and the use of pulse field gradients can further extend ^{1}H NMR's capabilities. Thus NMR is a

powerful technique to study membrane heterogeniety down to the 10's of nanometers, while for heterogeneities below 10's of nanomenters, other techniques such as inelastic X-ray scattering (IXS) and Förster resonance energy transfer (FRET) are better suited.

2.2.1 Solid State ^{2}H NMR

For lipids, ^{2}H can substitute ^{1}H as a minimally invasive probe, where the electric field gradient the nucleus experiences is primarily due to a carbon-deuterium bond. This orientationally dependent interaction broadens the line shape into a Pake powder pattern (62), which can experience narrowing due to motional averaging (see Fig. 4A). Therefore, the width of the line shape is proportional to an order parameter. Typically, the terminal acyl chain methyls in lipids experience the most disorder, thus possess the lowest order parameters – order parameters increase as one approaches the lipid/water interface. Note, that although using deuterium as a probe is minimally invasive compared many other molecular and atomic probes, per-deuterated lipids often have a solid-ordered to liquid-disordered phase transition a few degrees Celsius lower than their non-deuterated couterparts.(63) Nevertheless, deuteration seems to have a minimal effect on lipid phase separation(64), and the observed domain miscibility temperature observed by ^{2}H NMR is in agreement with flourscence microscopy results(65). (Note that fluorescent microscopy uses probes that can perturb the membrane in potentially the same way as deuterium labeling, so a lowering of the miscibility temperature should not be completely discounted.)

Solid state ^{2}H NMR's sensitivity to lipid order is very useful in detecting liquid-ordered and liquid-disordered phases. Prior to the formulation of the lipid raft hypothesis, solid state ^{2}H NMR was fundamental in establishing the properties of high-cholesterol, raft-like liquid ordered phases (66, 67). Veatch et. al studied domain formation in DOPC/DPPC-d_{62}/cholesterol mixtures, initially with 30 mol% cholesterol (65) and later using different lipid compositions and temperatures (68). At temperatures between 20 °C and 30 °C and 20 mol% cholesterol, Veatch et al. observed the superposition of methylene signals from both liquid-ordered and liquid-disordered phases, implying the presence of large domains and phase coexistence. Increasing the temperature past 30 °C, broadened the line shape, indicating the exchange of lipids between domains (65, 66, 69), although the authors suggested this could also have been the result of composition fluctuations (68). At low and high cholesterol concentrations, the presence of liquid-liquid domain phase coexistence was absent, implying that a moderate amount of cholesterol (20 mol%) is important for the formation of large liquid-liquid domains. These works contributed to reinforcing the importance of cholesterol in the formation and stabilization of lipid domains.

In addition to cholesterol, sphingomyelin has also been identified as an important lipid raft component (11). Bunge et. al studied the mixture POPC, PSM (palmitoyl sphingomyelin), cholesterol with perdeuterated *sn*-2 chain analogs of POPC and PSM (70). Using the methyl line width difference (from the POPC and PSM specrra) to calculate the exchange rate using Eq. 1 and diffusion distance from Eq. 2, they estimated domain sizes to be 70 nm, or smaller. Later Yasuda et. al studied the mixture of DOPC, SSM (steroyl sphingomyelin), cholesterol using selectively deuterated analogs of each component (71). Here, superposition of spectra for liquid-disordered and liquid-ordered domains were observed for each component. Fitting the different NMR line shapes, Yasuda et al. determined that approximately 80 mol% of SSM and cholesterol were in the liquid-ordered domain, while 60 mol% of DOPC was found in the liquid-disordered domain (71). The increased domain size due to the more disordered and thinner DOPC rich phase, compared to POPC (28), allowed Yasuda et al. to directly determine domain composition from NMR data (71).

A lesser studied aspect of domain formation is the influence of the liquid-disordered domain. Lipids containing acyl chains with multiple double-bonds such as, docosahexaenoic acid (DHA), eicosapentaenoic acid (EPA), and docosapentaenoic acid (DPA), belong to a class of naturally occurring, highly disordered lipids. For the aforementioned polyunsaturated fatty acids (PUFAs), it is understood that the double bonds cause packing defects within the membrane, which result in highly disordered phases. Their influence on liquid-ordered domain size is two-fold: (i) by increasing the thickness mismatch between domains; and (ii) sequestering cholesterol to the ordered domain (72). When comparing lipids with PUFA chains to those with monounsaturated acyl chains, it has been found that the order of the liquid-ordered phase is increased (73–75). In mixtures of SM and cholesterol with either PDPC (DHA containing lipid) or PEPC (EPA containing lipid), a superposition of signals by ^{2}NMR was observed (76, 77). In analyzing the spectra from these lipid mixtures, Williams et. al and Kinnun et. al used "dePaking" which allows the domain composition analysis to be improved for perdeuterated lipids (78). For both DHA and EPA, palmitoyl sphingomyelin (SM) and cholesterol were the major components making up the liquid-ordered domain, whereas PDPC had a greater propensity to enter the ordered domain than PEPC (76, 77). In the case of the PDPC/SM/cholesterol composition, a lower limit domain size was estimated to be around 40 nm in diameter based on separation of resonance frequencies in the cholesterol spectrum and using Eq. 2. The separation of resonance frequencies in the PDPC spectrum was narrower, thus it was estimated that the upper limit domain diameter was 100 nm, a value closer to the true domain size. Although ^{2}H NMR has its limits in accurately determining domain size, it is particularly relevant for determining domain composition.

As described, solid state ^{2}H NMR is a powerful technique used to observe the formation of liquid-liquid domains, estimating

their size and determining their compositions. In many ways, ^{2}H NMR complements SANS. Typically, lipids with perdeuterated acyl chains are more readily available than selectively deuterated lipids. However, since perdeuterated lipids produce a spectrum of superposed Pake powder patterns, the use of deconvolution techniques greatly simplifies their analysis (78). As a result, this opens up solid state ^{2}H NMR to studies of more biologically relevant and complex systems, such as the lipids found in *archaea* (79).

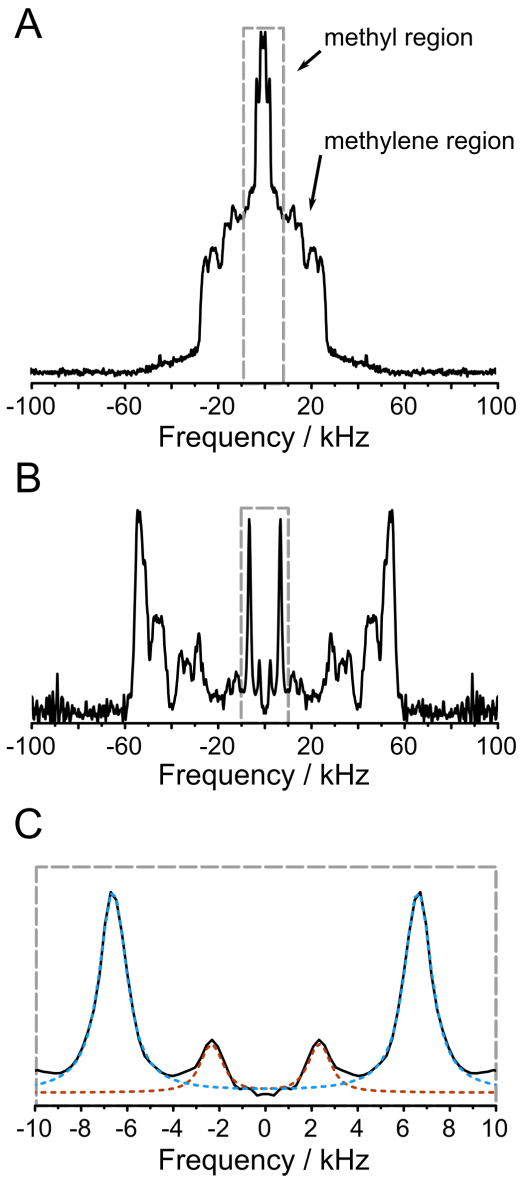

Figure 5: ^{2}H NMR spectra from PSM-d_{31}/PDPC/cholesterol bilayers can be analyzed by "dePaking" the spectra. The methyl resonances in each lipid domain can then be be fitted to determine domain composition (77). (A) Here, the palmitoyl chain of PSM is perdeuterated, thus the NMR spectrum appears as a superposition of symmetric "Pake" powder patterns, where the methyl resonances are the most disordered. (B) A "dePaking" deconvolution algorithm was used to convert the anisotropic Pake powder patterns to isotropic peaks (78). (C) The methyl region resonances for the liquid-disordered (inner pair of peaks) and liquid-ordered (outer peaks) phases were fitted to determine domain composition. The figure was adapted from Kinnun et. al.(77).

2.2.2 Magic Angle Spinning ^{1}H NMR

Although ^{1}H (a spin 1/2 nucleus) is naturally abundant in biomolecules, its NMR spectrum is somewhat featureless due to anisotropic interactions. This drawback is addressed by magic angle spinning (MAS), where the sample is rotated at high speeds at the so-called "magic angle" of 54.74°. Here, the anisotropic interactions are averaged and the spectral resonances are narrowed. Doing so, increases the sensitivity of MAS NMR, allowing for smaller sample sizes. As such, MAS NMR is particularly well suited for the study of ULVs that better approximate biological cells – solid state ^{2}H NMR is typically used to study multilamellar vesicles (MLVs). The formation of more ordered domains in the membrane, such as liquid-ordered domains, causes line widths to broaden (61). This is due to the increased strength of the inter-lipid dipolar interactions taking place amongst the protons, which are undergoing a slower rate of isomerization in the more ordered phases. Since there is a large difference in the line widths of the two phases, line shape analysis of the spectra can be used to detect the formation of nanometer-sized domains.

Veatch et. al used ^{1}H MAS NMR to observe domain formation in a mixture of DOPC/DPPC/cholesterol (65). The liquid-ordered (8 °C) and liquid-disordered (45 °C) spectra had sufficient differences in line shape width that they could be fitted at intermediate temperatures as a superposition of the different spectra. This allowed Veatch et al. to determine the percent of liquid-ordered and liquid-disordered phases as a function of temperature, and also determine the miscibility temperature. Later, Polozov et. al studied similar lipid mixtures, but with the addition of SOPC (61). However, they used chemical exchange to estimate domain sizes, which were determined to be at least 300 nm in size. Note, that this technique can be extended to naturally-abundant ^{13}C MAS NMR and has been used to study cholesterol-raft interactions (80, 81) – it should be pointed out, however, that ^{13}C MAS NMR is less sensitive than ^{1}H MAS NMR due to the lower natural abundance of ^{13}C. MAS NMR has also been extended to the ^{31}P nucleus, where Koukalová et al. used this technique, with other methods, to determine that the liquid-ordered domains in DOPC/SM/cholesterol mixtures were reminiscent of the liquid-disordered phase.(82). Recently, Warschawski et. al developed a multidimensional 31P MAS NMR techinque to enhance the studies of lipid dynamics in phase separated lipid membranes.(83) Beyond model membrane systems, MAS NMR has been used to detect the presence of lipid domains in living systems, such as the envelope of the influenza virus (84).

One should note that the NMR determination of domain size relies on knowledge of lipid diffusion, as shown by Eq. 2. Polozov et. al used pulse field MAS NMR to study domain formation and lipid diffusion in SOPC/POPE mixtures (85). Again, line width differences between the liquid-disordered and, in this case, solid ordered spectra, enabled Polozov and co-workers to determine the percent of liquid-disordered and solid-ordered domains. Specifically, they carried out diffusion measurements using a radio-frequency pulse which generated a magnetic field gradient across the sample (hence pulse field gradient). If no diffusion was taking place, the line shape would be broad due to the lipids occupying multiple locations. However, as diffusion increases, the signal width decreases – the signal intensity increases due to motional averaging. This allowed MAS NMR to determine lipid diffusion and consequently, domain size. At the time of the Polozov et al. studies, domain sizes down to 500 nm could theoretically be determined. However, currently with the use of larger pulse field gradients, nanometer sized domains can be realistically measured (86)(87).

2.3 Förster Resonance Energy Transfer (FRET)

Fluorophores have enabled techniques, in particular Förster or fluorescence resonance energy transfer (FRET), to observe the existence of lipid-lipid domains.(88, 89) Although the length scales accessible to common optical techniques are limited by the diffraction limit – ruling out the observation of nanoscopic domains (90) – FRET utilizes the energy transfer between donor and acceptor fluorophores to reveal structure on the nanoscale. The efficiency of energy transfer (nonradiative dipole–dipole coupling) between two fluorophores (FRET efficiency, E) decays rapidly as a function of distance – i.e., is inversely proportional to the sixth power of the distance separating the donor and acceptor fluorophores. Thus, only nearby donor and acceptor probes can participate in an efficient and measurable transfer of energy. Measurements of FRET efficiency can be used to determine if a FRET pair (donor and acceptor probes) is within a certain distance of each other.

In 2000, Stillwell et al. performed early FRET measurements on phase separating lipid mixtures containing PUFAs, saturated lipids, and cholesterol, using FRET pairs of varying acyl chains.(91) Small decreases in FRET efficiency were observed when the probes partially partitioned into liquid-ordered and liquid-disordered domains. Since full partitioning was not achieved, only small changes in FRET efficiency were observed. However the work by Stillwell et al. demonstrated that FRET was sensitive to liquid-liquid domain formation and showed that cholesterol promotes phase separation. A year later, Feigenson and Buboltz took into account the partitioning of the FRET probes in the different lipid phases and produced a much-used DPPC/DLPC/cholesterol phase diagram.(92) Since then, FRET has been used to determine the existence of nanodomains in a range of systems, including bacterial membranes(93) and living cells(94, 95).

FRET efficiency can be custom-tailored for studies of different domain sizes by controlling the properties of the FRET pair – FRET is often described as a "molecular ruler."(96–98) For example, Heberle et. al were able to use FRET to demonstrate

liquid-ordered domain formation in POPC, SOPC, DSPC, and cholesterol mixtures.(43) Based on the FRET pair used, they estimated domain size to be on the order 10 nm in diameter. In 2015, Priyadarshini et. al were able to refine the acceptor and donor probes to detect nanodomains down to approximately 2.6 nm. As noted by Stillwell et. al., donor and acceptor fluorophores do not completely partition between the liquid-disordered and liquid-ordered domains,(91) thus knowledge of partition coefficients is vital for the accurate determination of of domain sizes with FRET. Enoki et. al used multiple experiments to measure donor and acceptor probe partitioning and also carried out Monte Carlo simulations of different size domains. Doing so allowed them to associate FRET efficiencies with domain sizes of approximately 10 nanometers, or less.(99) Vinklárek et. al used a similar technique of combining FRET with Monte Carlo simulations. They were able to observe interleaflet coupling of nanodomains at a similar length scales.(100) Recently, Scott et. al published an analytical solution for determining domain size from FRET without the need of Monte Carlo simulations, increasing the accessibility of FRET.(101)

Given that FRET can tune its nanometer-scale sensitivity through the use of different donor and acceptor probes, it is able to detect the presence of heterogeneities at length scales well below most other techniques. This in addition to recent advances in data analysis methods will enable the FRET technique to study increasingly complex systems of interest to biologists.

3 EMERGENT TECHNIQUES

In addition to neutron scattering and NMR, there have been techniques that have provided us with much information regarding the static and dynamic structures of lipid domains. For example, over extended time scales, atomic force microscopy(102–105) and super-resolution fluorescence microscopy(106, 107) are two such techniques. Moreover, secondary ion mass spectrometry allows for lateral resolutions of approximately 100 nm, with the added ability of determining lipid domain composition (108). In the following section of this article we will discuss new techniques which we believe have the potential to provide complementary new insights into the static and dynamic structures of membranes, lipid domains, and emergent properties.

3.1 Inelastic X-ray Scattering

Non-resonant, high-resolution inelastic X-ray scattering (IXS) is a non-invasive technique capable of probing the atomic dynamics of crystalline, soft, and biological materials (109). Atomic dynamics in these materials exist in the form of quantized collective motions, i.e., phonons or normal modes, due to thermally triggered density-density fluctuations (110–113). Phonons were experimentally measured – for the first time – in metallic vanadium by Brockhouse using the then newly-developed triple-axis spectrometer (114) – he shared the 1994 Nobel Prize in physics for his inelastic studies of condensed matter (115). Moreover, inelastic neutron scattering (INS) has routinely been used to study phonon excitations in soft and biological materials, including phospholipid membranes (116). Despite the unique capabilities offered by neutron scattering techniques, such as contrast variation and selective deuteration, INS is kinematically (geometrically) restricted in accessing low energy-transfer and momentum-transfer phonons, as compared to IXS (117–119).

In IXS measurements (22, 120), an incident x-ray beam with energy E_i and momentum $\hbar\mathbf{k}_i$ scatters with energy E_f and momentum $\hbar\mathbf{k}_f$. Since phonons originate from thermally mediated density-density fluctuations, the scattered x-ray beam contains information about phonon excitations corresponding to the measured energy transfer $E = E_f - E_i$ and momentum transfer $\hbar\mathbf{Q} = \hbar\mathbf{k}_f - \hbar\mathbf{k}_i$ (22, 120), respectively. The measured IXS vibrational spectra can then be fitted using the Damped Harmonic Oscillator (DHO) model represented as:

$$\mathrm{DHO} = \sum_{l=0}^{N} \frac{A_l(Q)\Gamma_l(Q)E_l^2(Q)E^2}{(E^2 - E_l^2(Q))^2 + (\Gamma_l(Q)E)^2}, \tag{3}$$

where E_l is the average excitation energy, $A_l(Q)$ is the amplitude of a single inelastic ($E_l \neq 0$) phonon excitation, and $\Gamma_l(Q)$ is the half-width at half-maximum of a spectral feature (120). All selected IXS spectra have a certain number of phonon excitations over a measured energy-wavenumber (E-Q) range.

IXS has been successfully used to access longitudinal and transverse phonon excitations (acoustic and optical phonon modes, respectively) in soft materials, such as simple liquids (127, 128), block copolymers (129), colloids (130), and liquid crystals (mesogens) (131, 132). Importantly, Fig. 6 shows the first experimental evidence for the existence of transverse phonons and their low-(E, Q) phonon gap measured in DPPC membranes using IXS (121). Figure 6 (a) shows the IXS scattering geometry measuring in-plane collective lipid motions in time (picosecond) and length (nanometer). Figure 6 (b) shows phonon dispersions of gel (20 °C) and fluid (45 °C) phase DPPC bilayers. A transition from the gel to fluid phase leads to the emergence of the transverse (shear) (E, Q)-gap, implying that shear elastic waves are over damped beyond their nanometer length scale propagation. Furthermore, (E, Q)-gaps define viscoelastic crossovers in the vibrational spectra of biomembranes. In other words, at higher energies (frequencies) and higher Q-values, biomembranes are capable of supporting the propagation of

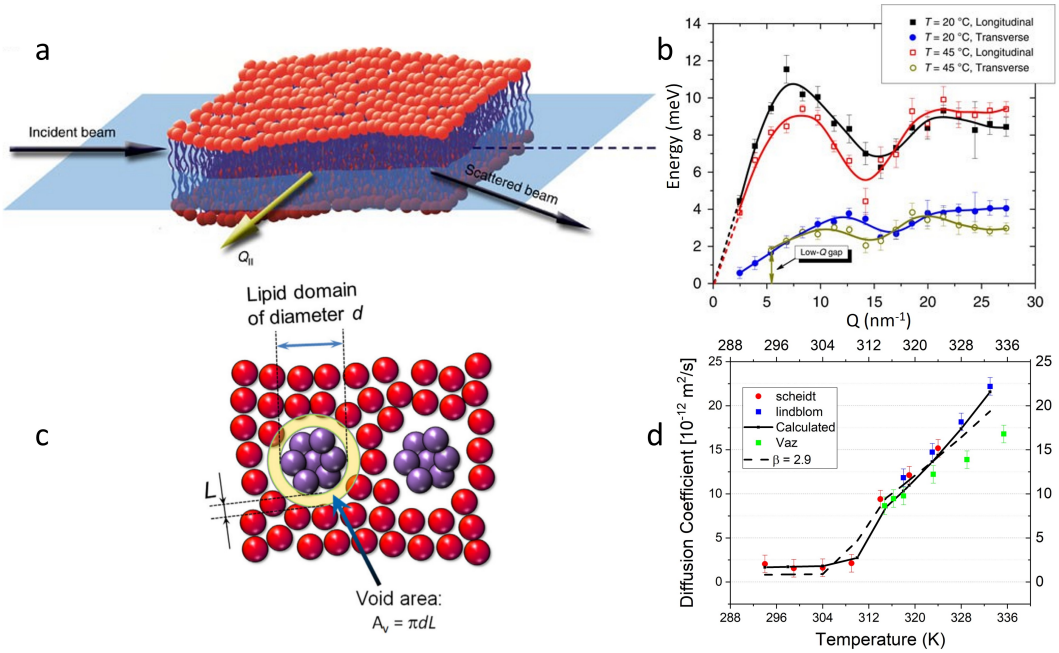

Figure 6: Experimental evidence for the emergent behavior of phonon (E, Q)-gaps in the vibrational spectra of lipid membranes as revealed by inelastic X-ray scattering (IXS). (a) Schematic of the IXS scattering geometry, where an incident x-ray beam scatters from a phospholipid membrane (121). (b) Longitudinal and transverse acoustic phonon excitations of a DPPC membrane at 20 °C (gel phase) and 45 °C (fluid phase) (121). (c) Schematic of a transient nanoscopic lipid domain surrounded by transient nanopores, effectively forming a transient void ring (122). The existence of transient void rings around transient lipid nanodomains across the membrane is responsible for the passive transmembrane transport of small molecules and solutes (122), molecular-level mechanical stress propagation (123), and self-diffusion of lipids (122). (d) The lateral self-diffusion coefficient $D(T)$ of a DPPC membrane calculated from Eq. (8) and compared with measured values (124–126) from different lipid phases (gel, ripple, and fluid) (122).

compression (longitudinal phonons) and shear waves (transverse phonons). In contrast, biomembranes lose their ability to support shear waves once (E, Q)-gap values are reached, thus, transitioning from the elastic to viscous regime. Therefore, (E, Q) phonon gaps define the size and lifetime of transient lipid nanodomains in biomembranes. For instance, an (E, Q)-gap emerges at 45 °C, see Figure (6 (b)), at about $E \simeq 2$ meV and $Q \simeq 5.2$ nm^{-1}. The lifetime of the transient lipid nanodomains can therefore be estimated as $\tau = \frac{E_{gap}}{\hbar}$ (~2.07 ps), and their size as $d = \frac{2\pi}{Q_{gap}}$ (~1.2 nm). This means that transient lipid nanodomains are essentially solid-like rattling domains surrounded by transient voids beyond ~1.2 nanometers during ~2.07 picoseconds (elastic regime), see Figure 6 (c). At longer times transient lipid nanodomains become viscous (viscous regime) – shear restoring forces are negligible – allowing lipids to self-diffuse around the transient void ring (123). It is worth noting that lipid raft boundaries may have fractal dimensions (133). Furthermore, the formation and dissolution of transient lipid nanodomains reiterates undergoing viscoelstic crossovers across the membrane in random places and at random times (123). In this regard, the vibrational landscape of biomembranes at picosecond time and nanometer length scales is reminiscent of the surface of a boiling liquid. As a result, the existence of (E, Q) phonon gaps is responsible for the molecular-level mechanical stress propagation in the form of compression waves (123), passive transmembrane transport of small molecules and solutes (121), and self-diffusion of lipids (22, 122), see Figure 6 (c). Below, we show how phonon gap parameters can be utilized to calculate self-diffusion coefficients, see Figure 6 (d).

Phonon excitations in biological membranes can also be studied through the calculation of the longitudinal $C_l(Q, E)$ and transverse $C_t(Q, E)$ current correlation spectra using molecular dynamics (MD) simulations (22, 122). Phonon modes and their dispersions can be calculated through the projection of lipid-lipid correlation functions in directions along and perpendicular to the wavevector $\vec{Q}$ (122). Current correlation spectra $C_\alpha(\vec{Q}, E)$ can be written as:

$$C_\alpha(\vec{Q}, E) \equiv \int_{-\infty}^{+\infty} dt\, e^{iEt} \langle \vec{J}^*_\alpha(\vec{Q}, t) \cdot \vec{J}_\alpha(\vec{Q}, t) \rangle, \tag{4}$$

where $\alpha = (l$ - longitudinal; t - transverse), and the corresponding time-dependent current-current correlation functions read as:

$$\vec{J}_l(\vec{Q},t) = \frac{1}{\sqrt{N}}\sum_m \hat{\vec{Q}}(\hat{\vec{Q}}\cdot\vec{v}_m(t))e^{-i\vec{Q}\cdot\vec{r}_m(t)} \quad (5)$$

$$\vec{J}_t(\vec{Q},t) = \frac{1}{\sqrt{N}}\sum_m \hat{\vec{Q}}\times\vec{v}_m(t)e^{-i\vec{Q}\cdot\vec{r}_m(t)}, \quad (6)$$

where $\hat{\vec{Q}}$ is the unit vector along $\vec{Q}$, N is the total number of molecules, and $\vec{r}_m(t)$ and $\vec{v}_m(t)$ are coordinates and velocities of molecule m, respectively. Thereafter, both longitudinal and transverse phonon modes of biomembranes, including their (E, Q) phonon gaps, can be readily obtained by fitting $C_l(Q,E)$ and $C_t(Q,E)$ using the DHO model (22, 122). Furthermore, the self-diffusion coefficient D_l can be written as:

$$D = \frac{k_B T}{f} e^{-\frac{A_r}{A_v}}, \quad (7)$$

where k_B is the Boltzmann constant, T is the temperature, f is the translational drag friction parameter (134), $A_r = \frac{\pi d^2}{4}$ is the area of a transient lipid nanodomain, $d = \frac{2\pi}{Q_{gap}}$ is the diameter of the transient void ring, Q_{gap} is the reciprocal space phonon gap, see Figure 6(b), $A_v = \pi dL$ is the area of the transient void ring around the transient lipid nanodomain. Finally, the temperature dependent self-diffusion coefficient can be represented as(122, 123):

$$D(T) = \frac{k_B T}{f} e^{-\frac{1}{2}\frac{\pi\beta(T)}{Qgap(T)R_l}}, \quad (8)$$

where β is the dimensionless displacement parameter of a lipid within the void ring, R_l is the van der Waals radius of a lipid, and L is the width of the transient void ring $\frac{R_l}{\beta}$, see Figure 6(c). In conclusion, Figure 6(d) shows a good agreement between the lateral self-diffusion coefficients calculated from Eq. (8), using phonon gaps as input parameters (122), and experimentally measured diffusion coefficients at different temperatures (124–126), spanning gel, ripple, and fluid phases (22, 122), validating the phonon theory of liquids and biological fluids (22).

3.2 Cryogenic Electron Microscopy

Although NMR, X-ray, and neutron scattering techniques are able to detect lipid domains that are below the wavelength of light microscopy (roughly 500 nm), they fail to produce real space images of lipid domains (135). Ideally, a technique that can detect nanoscopic lipid domains, but can also provide images of those domains can greatly advance our understanding of these structures, as seeing is believing. An emerging technique for lipid membrane biophysics that can achieve these two tasks is cryogenic electron microscopy (cyro-EM) (135, 136).

Electron microscopy (EM) was first developed in the 1930's, however, its' use for imaging biological samples was limited. To be imaged, samples must be dehydrated, placed in a vacuum, and exposed to high doses of electrons since biological samples have inherently low contrast to electrons (135, 136). Using glucose to "protect" their sample, Henderson et. al. used EM to determine the structure of bacteriorhodopsin, a large transmembrane protein containing seven alpha helices (137). A great advance to the study of biological materials by EM was the introduction of cryogenic stage that was able to maintain samples at near liquid nitrogen temperatures (138). A further improvement by Dubochet et al. was the flash freezing of samples by rapidly plunging them into liquid ethane, thereby vitrifying the water into an amorphous solid. This led to the development of what we now know as cryo-EM (139). However, it took two more important developments to realize the full potential of cryo-EM with regards to biological samples, those being the development of a new generation of direct electron detectors and advanced image-processing tools and algorithms to correct for sample movements and enable the reconstruction of 3D images from randomly oriented particles (135, 135, 136, 136). These developments enabled the measurement of biological samples under near native conditions, with increased contrast and a decreased susceptibility to radiation damage (135, 136).

Cryo-EM is rapidly becoming the "go-to" technique for structural biologists (135, 136). However, there have been very few cryo-EM studies specifically looking at the structure of lipid bilayers (140–142). Recently, Heberle et al. (143) and Cornell et al. (144) published cryo-EM studies of lipid domains, with each study using a different experimental approach. For example, Cornell et al. implemented cryo-electron tomography (cryo-ET) (136), which uses a series of different sample angle images to reconstruct a 3D image of the sample (144). A requirement of cryo-ET is that the sample is sufficiently thin to allow the transmission electrons (136). In contrast, Heberle et al. (143) used the single particle cryo-EM approach which generates a 3D reconstruction of the sample by combining a large number of 2D image projections of the same sample in different orientations. The studies by Heberle et. al. and Cornell et. al. both showed clear evidence of lipid domains, signifying the possible advent of cryo-EM as a potentially powerful technique for studying lipid domains in model lipid systems (143, 144).

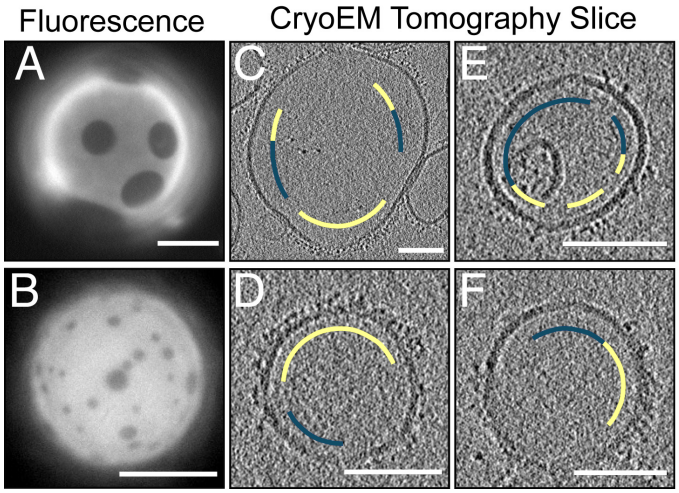

Figure 7: Imaging giant and large unilamellar vesicles (GUVs and LUVs, respectively) by fluorescence microscopy and cryo-ET using Trimeric his6-mcherry. (A-B) Fluorescence microscopy images of GUVs prepared with different lipid mixtures to tune the size of the lipid domains. Trimeric his6-mCherry was used to image lipid domains due to it's fluorescent properties. (C-F) Cryo-ET slices showing regions where trimeric his6-mCherry associates with the membrane (yellow) or where it is absent from the membrane (green). Here, trimeric his6-mCherry's electron dense properties were exploited in order to observe where the probe interacts with the membrane. Figure adapted from (144).

Using cryo-ET, Cornell et. al. studied lipid domains in a ternary lipid system containing DPPC/diphytanoyl phosphatidylcholine (DiPhyPC)/cholesterol, using two experimental approaches. The first used only cryo-ET to investigate the thickness mismatch between coexisting liquid disordered (Ld) and liquid ordered (Lo) domains in large unilamellar vesicles (LUVs). They compared the cryo-ET thickness results of six different lipid ratios along a tie line in the phase diagram of the lipid mixture of interest to fluorescence microscopy images of GUVs of the same lipid compositions. By comparing the area fractions of the Lo and Ld phases obtained from cyro-ET and fluorescence microscopy, Cornell et. al. determined that cryo-ET accurately identified submicron lipid domains in LUVs and that the area fractions of the two phases closely matched those from fluorescence microscopy. The second experimental approach used a probe, trimeric his6-mCherry, that was both fluorescent and electron dense, allowing the same GUV samples used in fluorescence microscopy to be extruded into LUVs for use in cryo-ET studies 7. From these complementary data sets, Cornell and co-workers concluded that cryo-EM was a valuable technique for the study of lipid nanostructures (144). Whether the vitrification process produces artifacts or not on domain structure has not been widely studied, however many of the aforementioned studies used complimentary techniques and discrepancies were not observed. This does not rule out the potential for artifacts, however for the systems studied if artifacts were present, they were minor.

Using single particle cryo-EM, Heberle et. al. (143) made use of both actual and simulated cyro-EM images to determine the thicknesses of single component lipid bilayers, phase separated bilayers, and cell-derived PMs. Using LUVs composed of PC lipids with monounsaturated diacyl chains ranging in length from 14 to 22 carbons, Heberle et. al. compared membrane thickness values from cryo-EM with those from small angle X-ray scattering (SAXS) and all-atom simulations. The bilayer thickness determined from cryo-EM (the distance between the two dark concentric rings in an LUV, which they referred to as the trough-to-trough distance (D_{TT})) agreed well with the hydrophobic thickness ($2D_C$) determined from SAXS data. In addition, bilayer thicknesses determined from simulated cryo-EM images were compared to thicknesses from all-atom simulations and it was again determined that the best agreement between thicknesses was $2D_C$.

Using the ternary system of DPPC/dioleoyl phosphatidylcholine (DOPC)/cholesterol, Heberle et. al. clearly showed the presence of regions with differing thickness within the same LUV, which would correspond to the Lo and Ld phases, similar to what was shown by Cornell et. al (144) (Figure 8). From the analysis of the images, it was found that there was a thickness difference in D_{TT} of 6.3 Å between the Lo and Ld phases, consistent with previous measurements of the same system. Finally, Heberle et. al. (143) showed the presence of nanoscale heterogeneities in giant plasma membrane vesicles (GPMVs) isolated from rat basophilic leukemia (RBL) cells. Two different thickness distributions in D_{TT} centered at 37.3 Å and 33 Å were determined from the cryo-EM images. The thicker distribution was comparable to D_{TT} values obtain from the Lo phase in the ternary mixture, whereas the the thinner region lay between the D_{TT} values for the Lo and Ld phases in the ternary mixture.

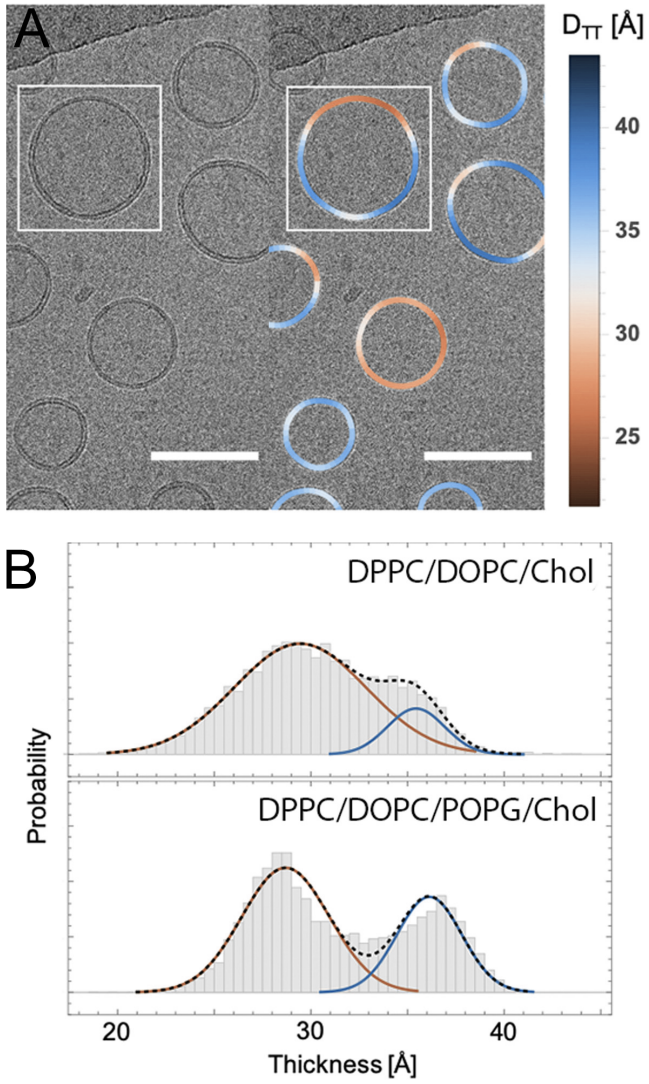

Figure 8: Visualization of lipid domains using Cryo-EM. (A) LUVs composed of DPPC/DOPC/palmitoyl oleoyl phosphatidaglycerol (POPG)/cholesterol (40/35/5/20) showing clear variations in membrane thickness (D_{TT}) visually (left) or by color coding (right), where the blue shading indicates regions with a thicker membrane. The scale bar is 100 nm. (B) Histograms showing the thickness distributions of two different lipid domain forming membrane compositions, DPPC/DOPC/cholesterol (40/40/20) (top) or DPPC/DOPC/POPG/cholesterol (40/35/5/20) (bottom). It was observed that the inclusion of POPG, a negatively charged lipid commonly used to prevent MLV contamination in extruded samples (140), enhances the separation between the two bilayer thickness distributions. Figure adapted from (143).

4 FUTURE TECHNIQUES

As technology advances more techniques will emerge to reveal a more nuanced picture of nanodomains. Here describe two such techniques, namely neutron reflectometry and droplet interface bilayers (DIBs).

4.1 Neutron Reflectometry

While SANS detects scattered neutrons at small angles, neutron reflectometry (NR) deals with reflected neutrons. The geometry of an NR experiment, shown in Figure 9, lends itself to investigations of hierarchical structures, such as domains in model membrane systems. Although it can be difficult to detect nanometer-sized structures in the lateral direction using NR, it is well-suited to detecting changes in depth, such as bilayer asymmetry and thickness. In general the resolution along the thickness of the membrane can approach 5Å, while the in-plane resolution is on the order of microns. Therefore, most studies focus on

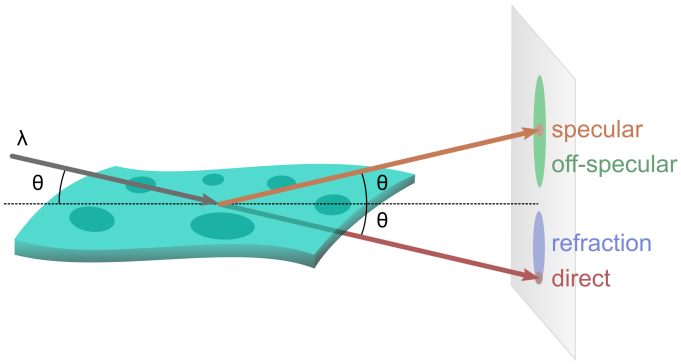

Figure 9: Geometry of a reflectometry experiment highlighting some of the scattered components from a membrane projected onto the plane of the detector. For a given measurement, either the incident angle θ is fixed with a varying λ or *vice versa*. The neutrons then interact with the membrane with one of four outcomes shown. (i) The neutrons are unaffected impinging directly on the detector, labeled direct; (ii) The neutrons refract, landing between the direct spot and the sample horizon; (iii) The neutrons specularly reflect at an angle of incidence θ. The specular reflections are dominated by chemical order along the thickness of the membrane; and (iv) the neutrons reflect at an angle that differs from the incident angle θ and above the sample horizon. In this scenario, the signal is dominated by lateral correlations of the membrane, such as the distribution and possible ordering of lipid domains.

the extraction the depth dependent scattering length density (SLD) which can be related to the laterally averaged chemical composition (32, 145–148). Reference layer techniques can be used to improve the quality of the depth dependent SLD extracted through model fitting (146), or the reciprocal scattering data can be directly inverted to a real space scattering SLD profile (149, 150). Note that the study of membranes with NR generally requires a substrate support which has an effect on lipid structure, diffusion, and dynamics, however by adjusting the substrate coating or by using a polymer cushion the effect of the support can be substantially reduced.(151–153) Also note that, many living cells support their membranes by a cytoskeleton which may have similar effects on the membrane as using a substrate.

NR is particularly powerful in determining the redistribution of membrane biomolecules across asymmetric membranes. Interpreting the SLD in the direction perpendicular to the bilayer normal (z) has shown to be sufficient when studying asymmetric model membranes (154), protein structures embedded in model membranes (145), molecules absorbed to the membrane surface, and material transport across the model membrane (155). Important to structure, Rondelli et. al found that ganglioside GM1 (monosialotetrahexosylganglioside) in lipid bilayers causes cholesterol to redistribute to GM1 deficient leaflets (156). Studies that rely on the off-specular signal from membrane systems are few, even though most modern instruments will measure both the specular and off-specular signal simultaneously on either a linear or area detector. Potential causes may include the lack of long range in-plane order that can push the signal of interest below the noise floor. It should also be noted that lipid rafts may be transient. However, by using asymmetric membranes, the redistribution of lipids (including raft constituents) can be studied with NR. Note that NR takes advantage of contrast matching in the same way other neutron scattering techniques do. Thus it has the ability to selectively contrast lipid species and thus domains. Since its strength is determining thicknesses it has the potential to determine the thicknesses of each domain independently, in the same system, with high accuracy.

4.2 Capacitive Detection of Nanoscale Domains

Cooperative, first-order phase transitions in model membranes consisting of one to a few components have been thoroughly characterized from temperature-dependent calorimetry, densitometry, and fluorescence experiments. However, thermotropic transitions in eukaryotic membranes containing numerous lipid species and high concentrations of cholesterol have remained undetectable using these techniques.(157)

Specific capacitance, C_M, defined as the electrical capacitance per unit area, is an intrinsic membrane property that is proportional to the dielectric permittivity and inversely proportional to the bilayer's thickness (158–160). Because acyl chain composition and orientation in the membrane affect permittivity and thickness, C_M is directly influenced by composition and thermotropic phase. While many studies have shown that electrical capacitance is sensitive to thermally induced lipid phase transitions in single-component model membranes (161–166), few capacitance measurements have been reported for lipid mixtures. Capacitance measurements conducted on multi-component cholesterol containing mixtures can provide tractable models of phase separation and lipid raft formation across a range of spatial length scales. As such, there is yet untapped

potential to use capacitance measurements for examining thermal transitions occurring in multi-component membranes that more closely reflect the lipid heterogeneity found in cells.

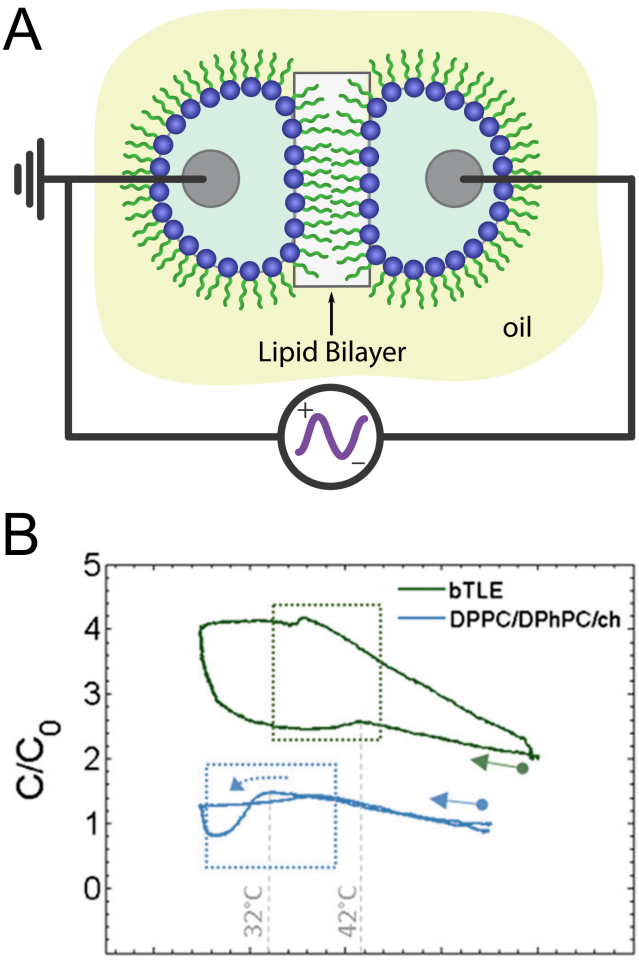

Figure 10: (A) The droplet interface bilayer (DIB) technique is composed of two aqueous lipid droplets suspended in oil in which their point of contact forms a lipid bilayer. Electrodes in each droplet allows for resistance and capacitance measurements. (B) Capacitance and temperature curves from cooling DPPC/DPhPC/Chol (20/50/30 mol %) and bTLE DIBs (C16 alkane solvent) reveal low-enthalpy phase transitions. Here the starting point of the cooling leg is indicated by arrows with circular end points while the cooling leg of the response is indicated by dashed arrows.

Temperature-dependent electrical capacitance measurements have been performed in planar bilayers composed of synthetic single or three-component lipid mixtures, or of natural brain total lipid extract (bTLE), which is rich in high-melting lipids, such as sphingomyelins, low-melting mixed-chain lipids, and cholesterol. The droplet interface bilayer (DIB) technique(167) was used to construct stable lipid bilayers between lipid-coated water droplets immersed in alkane oils. DIBs were perpared by suspending two aqueous lipid droplets attached to Ag/AgCl electrodes in an alkane oil reservoir with a lipid monolayer forming at the water-oil interface, where the lipid headgroups interact with water and the acyl chains protrude into the oil phase. Formation occurs when two droplets are pushed together, allowing the acyl chains of the individual droplets to interact with each other, forming a lipid bilayer as shown in fig. 10A. Not all lipid mixtures form DIBs, it is particularly difficult to form DIBs of lipids in the gel phase, however some techniques such as heating to high temperatures then cooling have proven successful in DIBs formation for difficult systems.(168) In general, DIBs are well-suited for electrical capacitance measurements because they allow independent measurements of nominal membrane capacitance and bilayer area (i.e. contact area between two droplets), thereby enabling a precise determination of C_M (169, 170). In addition to the familiar first-order thermotropic transitions in single component lipid membranes, capacitive measurements have identified transitions in mixed-lipid membranes that were not detected with one or more standard techniques, including calorimetry, densitometry, fluorescence microscopy, and Förster

resonance energy transfer spectroscopy. For example, capacitance measurements of bTLE bilayers indicated a phase transition at 38°C, shown in Fig. 10B, that could not be seen with any other method. These results indicate that electrical capacitance in DIBs can detect entropic membrane transitions specifically, due to its extreme sensitivity to variations in bilayer thickness.

First-order, thermotropic transitions in simple, single-component lipid membranes involve large scale structural changes that result in destabilizing defects and unwanted conductive pore formation. Capacitance measurements have been used to detect and corroborate thermotropic melting and miscibility transitions, but they have also been able to detect more subtle temperature controlled structural rearrangements in membranes comprised of mixtures of synthetic or natural lipids that can undergo transitions that are undetectable by standard methods. The sensitivity of capacitance measurements to low-enthalpy, higher-order phase transitions is a result of the inverse relationship between capacitance and hydrophobic thickness, whereby small changes in thickness can result in large changes in capacitance (171). Low-enthalpy, higher-order phase transitions detected with capacitance may control membrane structure at the nanoscale more smoothly, without high-amplitude thermal fluctuations and defect formation that occur in simpler model lipid membranes (172–175).

5 CONCLUSION

Over the past 100 years we have gained much insight into the static and dynamic structures of biological membranes and their emergent behaviors. Lipids were identified early on as the underlying structure of biological membranes and since then, membranes have evolved to include other biomolecules (e.g., proteins, carbohydrates, etc.). The proposal of lipid domains as functional supramolecular structures within the PM resulted in much controversy, and it has taken almost 30 years for the existence of lipid domains to be widely accepted by the scientific community.

As discussed, although neutron scattering and NMR techniques are well suited for the study of static and dynamic structures on the nanoscale, they were not widely used by the community studying lipid domains. This was due, in part, to the isotopic labeling requirements needed to fully enable these techniques, making it especially difficult to study *invivo* systems. Alongside these techniques, FRET has also emerged to study nanoscopic domains, capable of reaching of length scales in the few nanometers. For all of these techniques we described a number of *invitro* and *invivo* which detailed the existence of nanoscopic lipid domains.

Most recently, techniques such as IXS and cryo-EM are showing great potential in the study of the static and dynamic structures of nanometer sized lipid domains. For example, IXS has been used to access fundamental picosecond time and nanometer length scales to measure membrane viscoelasticity, molecular-level mechanical stress propagation, and self-diffusion of lipids. Cryo-EM has brought the ability to visualize nanometer sized domains, as well as thickness differences between domains and their surround in a relatively probe-free manner.

Finally, we discussed a couple of techniques, namely NR and DIBs that can be used in the future to provide us with complementary information regarding lipid domains. Although NR is widely used to study the structure perpendicular to the plane of the membrane (e.g., bilayer thickness), it has great potential to reveal unique details of the membrane's lateral organization. To do so, however, much work is needed to develop the appropriate theories to analyze the data and to increase the signal-to-noise ratio originating from the in-plane structures populating the membrane. The DIB technique, on the other hand, is particularly sensitive to the electrical properties of lipid membranes and its potential in membrane studies is far from being realized.

AUTHOR CONTRIBUTIONS

All authors contributed equally to this work.

DECLARATION OF INTEREST

The authors declare no competing interests.

ACKNOWLEDGMENTS

D.B. is supported through the National Science Foundation, Division of Molecular and Cellular Biosciences (MCB), under contract no. 2219289. J.K., T.R.C., and C.P.C. are supported through the Scientific User Facilities Division of the DOE Office of Basic Energy Sciences (BES), under contract no. DE-AC05 00OR2275. This review is dedicated to Klaus Gawrisch, which highlights his great contributions to the study of membrane biophysics with NMR. J.J.K. thanks Klaus Gawrisch for encouraging him during the early stages of his career.

REFERENCES

1. Overton, E., 1899. The probable origin and physiological significance of cellular osmotic properties. *Vierteljahrschrift der Naturforschende Gesselschaft (Zurich)* 44:88–135.

2. Pockels, A., 1892. On the relative contamination of the water-surface by equal quantities of different substances. *Nature* 46:418–419.

3. Langmuir, I., 1917. The constitution and fundamental properties of solids and liquids. II. Liquids. *Journal of the American chemical society* 39:1848–1906.

4. Gorter, E., and F. Grendel, 1925. On bimolecular layers of lipoids on the chromocytes of the blood. *The Journal of experimental medicine* 41:439.

5. Danielli, J. F., and H. Davson, 1935. A contribution to the theory of permeability of thin films. *Journal of cellular and comparative physiology* 5:495–508.

6. Singer, S. J., and G. L. Nicolson, 1972. The Fluid Mosaic Model of the Structure of Cell Membranes: Cell membranes are viewed as two-dimensional solutions of oriented globular proteins and lipids. *Science* 175:720–731.

7. Nicolson, G. L., 1976. Transmembrane control of the receptors on normal and tumor cells: I. Cytoplasmic influence over cell surface components. *Biochimica et Biophysica Acta (BBA)-Reviews on Biomembranes* 457:57–108.

8. Klausner, R., K. RD, K. AM, H. RL, and K. MJ, 1980. Lipid domains in membranes: evidence derived from structural perturbations induced by free fatty acids and lifetime heterogeneity analysis. *J. Biol. Chem.* .

9. Karnovsky, M. J., A. M. Kleinfeld, R. L. Hoover, and R. D. Klausner, 1982. The concept of lipid domains in membranes. *The Journal of cell biology* 94:1–6.

10. Simons, K., and S. D. Fuller, 1985. Cell surface polarity in epithelia. *Annual review of cell biology* 1:243–288.

11. Simons, K., and E. Ikonen, 1997. Functional rafts in cell membranes. *nature* 387:569–572.

12. Knoll, M., and E. Ruska, 1932. Das elektronenmikroskop. *Zeitschrift für physik* 78:318–339.

13. Borries, B. v., and E. Ruska, 1933. Die Abbildung durchstrahlter Folien im Elektronenmikroskop. *Zeitschrift für Physik* 83:187–193.

14. JD, R., 1960. The molecular structure and contact relationships of cell membranes. *Progress in biophysics and molecular biology* 10:343–418.

15. Kinnun, J. J., D. Bolmatov, M. O. Lavrentovich, and J. Katsaras, 2020. Lateral heterogeneity and domain formation in cellular membranes. *Chemistry and Physics of Lipids* 232:104976.

16. van Meer, G., E. Stelzer, R. W. Wijnaendts-van Resandt, and K. Simons, 1987. Sorting of sphingolipids in epithelial (Madin-Darby canine kidney) cells. *The Journal of cell biology* 105:1623–1635.

17. Heerklotz, H., 2002. Triton promotes domain formation in lipid raft mixtures. *Biophysical journal* 83:2693–2701.

18. Schuck, S., M. Honsho, K. Ekroos, A. Shevchenko, and K. Simons, 2003. Resistance of cell membranes to different detergents. *Proc. Natl. Acad. Sci. U. S. A.* 100:5795–5800.

19. Staneva, G., M. Seigneuret, K. Koumanov, G. Trugnan, and M. I. Angelova, 2005. Detergents induce raft-like domains budding and fission from giant unilamellar heterogeneous vesicles: a direct microscopy observation. *Chem. Phys. Lipids* 136:55–66.

20. Levental, I., K. R. Levental, and F. A. Heberle, 2020. Lipid rafts: controversies resolved, mysteries remain. *Trends Cell Biol.* 30:341–353.

21. Pike, L. J., 2006. Rafts defined: a report on the Keystone Symposium on Lipid Rafts and Cell Function. *Journal of lipid research* 47:1597–1598.

22. Bolmatov, D., 2022. The Phonon Theory of Liquids and Biological Fluids: Developments and Applications. *Journal of Physical Chemistry Letters* 13:7121–7129.

23. Kusumi, A., I. Koyama-Honda, and K. Suzuki, 2004. Molecular dynamics and interactions for creation of stimulation-induced stabilized rafts from small unstable steady-state rafts. *Traffic* 5:213–230.

24. Elson, E. L., E. Fried, J. E. Dolbow, and G. M. Genin, 2010. Phase separation in biological membranes: integration of theory and experiment. *Annu. Rev. Biophys.* 39:207.

25. Chadwick, J., 1932. Possible existence of a neutron. *Nature* 129:312–312.

26. Sears, V. F., 1992. Neutron scattering lengths and cross sections. *Neutron news* 3:26–37.

27. Jacrot, B., 1976. The study of biological structures by neutron scattering from solution. *Reports on progress in physics* 39:911.

28. Heberle, F. A., R. S. Petruzielo, J. Pan, P. Drazba, N. Kučerka, R. F. Standaert, G. W. Feigenson, and J. Katsaras, 2013. Bilayer thickness mismatch controls domain size in model membranes. *Journal of the American Chemical Society* 135:6853–6859.

29. Nickels, J. D., X. Cheng, B. Mostofian, C. Stanley, B. Lindner, F. A. Heberle, S. Perticaroli, M. Feygenson, T. Egami, R. F. Standaert, et al., 2015. Mechanical properties of nanoscopic lipid domains. *Journal of the American Chemical Society* 137:15772–15780.

30. Nickels, J. D., S. Chatterjee, C. B. Stanley, S. Qian, X. Cheng, D. A. Myles, R. F. Standaert, J. G. Elkins, and J. Katsaras, 2017. The in vivo structure of biological membranes and evidence for lipid domains. *PLoS biology* 15:e2002214.

31. Kinnun, J. J., H. L. Scott, R. Ashkar, and J. Katsaras, 2021. Biomembrane structure and material properties studied with neutron scattering. *Frontiers in chemistry* 9:203.

32. Lakey, J. H., N. Paracini, and L. A. Clifton, 2022. Exploiting neutron scattering contrast variation in biological membrane studies. *Biophysics Reviews* 3:021307.

33. Cusack, S., A. Miller, P. Krijgsman, and J. Mellema, 1981. An investigation of the structure of alfalfa mosaic virus by small-angle neutron scattering. *Journal of molecular biology* 145:525–543.

34. Timmins, P., J. Witz, et al., 1982. A neutron scattering study of the structure of compact and swollen forms of southern bean mosaic virus. *Virology* 119:42–50.

35. Kuzmanovic, D. A., I. Elashvili, C. Wick, C. O'Connell, and S. Krueger, 2003. Bacteriophage MS2: molecular weight and spatial distribution of the protein and RNA components by small-angle neutron scattering and virus counting. *Structure* 11:1339–1348.

36. Pencer, J., T. Mills, V. Anghel, S. Krueger, R. M. Epand, and J. Katsaras, 2005. Detection of submicron-sized raft-like domains in membranes by small-angle neutron scattering. *The European Physical Journal E* 18:447–458.

37. Pencer, J., T. T. Mills, N. Kučerka, M.-P. Nieh, and J. Katsaras, 2007. Small-angle neutron scattering to detect rafts and lipid domains. *In* Lipid Rafts, Springer, 231–244.

38. Anghel, V. N., D. Bolmatov, and J. Katsaras, 2018. Models for randomly distributed nanoscopic domains on spherical vesicles. *Physical Review E* 97:062405.

39. Bolmatov, D., W. T. McClintic, G. Taylor, C. B. Stanley, C. Do, C. P. Collier, Z. Leonenko, M. O. Lavrentovich, and J. Katsaras, 2019. Deciphering melatonin-stabilized phase separation in phospholipid bilayers. *Langmuir* 35:12236–12245.

40. Anghel, V. N., D. Bolmatov, J. Katsaras, and J. Pencer, 2019. Domains on a sphere: neutron scattering, models, and mathematical formalism. *Chemistry and Physics of Lipids* 222.

41. Bolmatov, D., M. Lavrentovich, and R. J. Reiter, 2022. Molecular interactions of melatonin with lipid rafts. *Melatonin Research* 5:101–113.

42. Zhao, J., J. Wu, F. A. Heberle, T. T. Mills, P. Klawitter, G. Huang, G. Costanza, and G. W. Feigenson, 2007. Phase studies of model biomembranes: complex behavior of DSPC/DOPC/cholesterol. *Biochimica et Biophysica Acta (BBA)-Biomembranes* 1768:2764–2776.

43. Heberle, F. A., J. Wu, S. L. Goh, R. S. Petruzielo, and G. W. Feigenson, 2010. Comparison of three ternary lipid bilayer mixtures: FRET and ESR reveal nanodomains. *Biophysical journal* 99:3309–3318.

44. Kuzmin, P. I., S. A. Akimov, Y. A. Chizmadzhev, J. Zimmerberg, and F. S. Cohen, 2005. Line tension and interaction energies of membrane rafts calculated from lipid splay and tilt. *Biophysical journal* 88:1120–1133.

45. Sur, B., R. Rogge, R. Hammond, V. Anghel, and J. Katsaras, 2001. Atomic structure holography using thermal neutrons. *Nature* 414:525–527.

46. Christensen, H., N. J. Garton, R. W. Horobin, D. E. Minnikin, and M. R. Barer, 1999. Lipid domains of mycobacteria studied with fluorescent molecular probes. *Molecular microbiology* 31:1561–1572.

47. Matsumoto, K., J. Kusaka, A. Nishibori, and H. Hara, 2006. Lipid domains in bacterial membranes. *Molecular microbiology* 61:1110–1117.

48. Epand, R. M., and R. F. Epand, 2009. Lipid domains in bacterial membranes and the action of antimicrobial agents. *Biochimica et Biophysica Acta (BBA)-Biomembranes* 1788:289–294.

49. Mileykovskaya, E., and W. Dowhan, 2000. Visualization of phospholipid domains in Escherichia coli by using the cardiolipin-specific fluorescent dye 10-N-nonyl acridine orange. *Journal of bacteriology* 182:1172–1175.

50. Kawai, F., M. Shoda, R. Harashima, Y. Sadaie, H. Hara, and K. Matsumoto, 2004. Cardiolipin domains in Bacillus subtilis marburg membranes. *Journal of bacteriology* 186:1475–1483.

51. Russell, R. A., P. J. Holden, K. L. Wilde, C. J. Garvey, K. M. Hammerton, and L. J. R. Foster, 2008. In vivo deuteration strategies for neutron scattering analysis of bacterial polyhydroxyoctanoate. *European Biophysics Journal* 37:711–715.

52. Ünnep, R., G. Nagy, M. Markó, and G. Garab, 2014. Monitoring thylakoid ultrastructural changes in vivo using small-angle neutron scattering. *Plant Physiology and Biochemistry* 81:197–207.

53. Nagy, G., and G. Garab, 2021. Neutron scattering in photosynthesis research: recent advances and perspectives for testing crop plants. *Photosynthesis research* 150:41–49.

54. Stingaciu, L.-R., H. O'Neill, M. Liberton, V. S. Urban, H. B. Pakrasi, and M. Ohl, 2016. Revealing the dynamics of thylakoid membranes in living cyanobacterial cells. *Scientific reports* 6:1–6.

55. Mezei, F., 1972. Neutron spin echo: A new concept in polarized thermal neutron techniques. *Zeitschrift für Physik A Hadrons and nuclei* 255:146–160.

56. MacKerell Jr, A. D., D. Bashford, M. Bellott, R. L. Dunbrack Jr, J. D. Evanseck, M. J. Field, S. Fischer, J. Gao, H. Guo, S. Ha, et al., 1998. All-atom empirical potential for molecular modeling and dynamics studies of proteins. *The journal of physical chemistry B* 102:3586–3616.

57. Himbert, S., A. D'Alessandro, S. M. Qadri, M. J. Majcher, T. Hoare, W. P. Sheffield, M. Nagao, J. F. Nagle, and M. C. Rheinstädter, 2022. The bending rigidity of the red blood cell cytoplasmic membrane. *PLOS ONE* 17:1–20.

58. Gerlach, W., and O. Stern, 1922. Der experimentelle nachweis der richtungsquantelung im magnetfeld. *Zeitschrift für Physik* 9:349–352.

59. Rabi, I. I., J. R. Zacharias, S. Millman, and P. Kusch, 1938. A new method of measuring nuclear magnetic moment. *Phys. Rev.* 53:318.

60. Ernst, R. R., and W. A. Anderson, 1966. Application of Fourier transform spectroscopy to magnetic resonance. *Rev. Sci. Instrum.* 37:93–102.

61. Polozov, I. V., and K. Gawrisch, 2006. Characterization of the liquid-ordered state by proton MAS NMR. *Biophys. J.* 90:2051–2061.

62. Pake, G. E., 1948. Nuclear resonance absorption in hydrated crystals: fine structure of the proton line. *J. Chem. Phys.* 16:327–336.

63. Bryant, G., M. B. Taylor, T. A. Darwish, A. M. Krause-Heuer, B. Kent, and C. J. Garvey, 2019. Effect of deuteration on the phase behaviour and structure of lamellar phases of phosphatidylcholines–deuterated lipids as proxies for the physical properties of native bilayers. *Colloids Surf. B* 177:196–203.

64. Li, L., H. Wang, and J.-X. Cheng, 2005. Quantitative coherent anti-Stokes Raman scattering imaging of lipid distribution in coexisting domains. *Biophys. J.* 89:3480–3490.

65. Veatch, S. L., I. Polozov, K. Gawrisch, and S. L. Keller, 2004. Liquid domains in vesicles investigated by NMR and fluorescence microscopy. *Biophys. J.* 86:2910–2922.

66. Vist, M. R., and J. H. Davis, 1990. Phase equilibria of cholesterol/dipalmitoylphosphatidylcholine mixtures: deuterium nuclear magnetic resonance and differential scanning calorimetry. *Biochemistry* 29:451–464.

67. Thewalt, J. L., and M. Bloom, 1992. Phosphatidylcholine: cholesterol phase diagrams. *Biophys. J.* 63:1176–1181.

68. Veatch, S. L., O. Soubias, S. L. Keller, and K. Gawrisch, 2007. Critical fluctuations in domain-forming lipid mixtures. *PNAS USA* 104:17650–17655.

69. Hsueh, Y.-W., K. Gilbert, C. Trandum, M. Zuckermann, and J. Thewalt, 2005. The effect of ergosterol on dipalmitoylphosphatidylcholine bilayers: a deuterium NMR and calorimetric study. *Biophys. J.* 88:1799–1808.

70. Bunge, A., P. Müller, M. Stöckl, A. Herrmann, and D. Huster, 2008. Characterization of the ternary mixture of sphingomyelin, POPC, and cholesterol: support for an inhomogeneous lipid distribution at high temperatures. *Biophys. J.* 94:2680–2690.

71. Yasuda, T., H. Tsuchikawa, M. Murata, and N. Matsumori, 2015. Deuterium NMR of raft model membranes reveals domain-specific order profiles and compositional distribution. *Biophys. J.* 108:2502–2506.

72. Wassall, S. R., and W. Stillwell, 2008. Docosahexaenoic acid domains: the ultimate non-raft membrane domain. *Chem. Phys. Lipids* 153:57–63.

73. Huster, D., K. Arnold, and K. Gawrisch, 1998. Influence of docosahexaenoic acid and cholesterol on lateral lipid organization in phospholipid mixtures. *Biochemistry* 37:17299–17308.

74. Shaikh, S. R., A. C. Dumaual, A. Castillo, D. LoCascio, R. A. Siddiqui, W. Stillwell, and S. R. Wassall, 2004. Oleic and docosahexaenoic acid differentially phase separate from lipid raft molecules: a comparative NMR, DSC, AFM, and detergent extraction study. *Biophys. J.* 87:1752–1766.

75. Soni, S. P., D. S. LoCascio, Y. Liu, J. A. Williams, R. Bittman, W. Stillwell, and S. R. Wassall, 2008. Docosahexaenoic acid enhances segregation of lipids between raft and nonraft domains: 2H-NMR study. *Biophys. J.* 95:203–214.

76. Williams, J. A., S. E. Batten, M. Harris, B. D. Rockett, S. R. Shaikh, W. Stillwell, and S. R. Wassall, 2012. Docosahexaenoic and eicosapentaenoic acids segregate differently between raft and nonraft domains. *Biophys. J.* 103:228–237.

77. Kinnun, J. J., R. Bittman, S. R. Shaikh, and S. R. Wassall, 2018. DHA modifies the size and composition of raftlike domains: a solid-state 2H NMR study. *Biophys. J.* 114:380–391.

78. McCabe, M. A., and S. R. Wassall, 1997. Rapid deconvolution of NMR powder spectra by weighted fast Fourier transformation. *Solid State Nucl. Magn. Reson.* 10:53–61.

79. Brownholland, D. P., G. S. Longo, A. V. Struts, M. J. Justice, I. Szleifer, H. I. Petrache, M. F. Brown, and D. H. Thompson, 2009. Phase separation in binary mixtures of bipolar and monopolar lipid dispersions revealed by 2H NMR spectroscopy, small angle x-ray scattering, and molecular theory. *Biophys. J.* 97:2700–2709.

80. Fritzsching, K. J., J. Kim, and G. P. Holland, 2013. Probing lipid–cholesterol interactions in DOPC/eSM/Chol and DOPC/DPPC/Chol model lipid rafts with DSC and 13C solid-state NMR. *BBA-Biomembranes* 1828:1889–1898.

81. Löser, L., K. Saalwächter, and T. M. Ferreira, 2018. Liquid–liquid phase coexistence in lipid membranes observed by natural abundance 1 H–13 C solid-state NMR. *Phys. Chem. Chem. Phys.* 20:9751–9754.

82. Koukalová, A., M. Amaro, G. Aydogan, G. Gröbner, P. T. Williamson, I. Mikhalyov, M. Hof, and R. Šachl, 2017. Lipid driven nanodomains in giant lipid vesicles are fluid and disordered. *Sci. Rep.* 7:1–12.

83. Warschawski, D. E., A. A. Arnold, and I. Marcotte, 2018. A new method of assessing lipid mixtures by 31P magic-angle spinning NMR. *Biophys. J.* 114:1368–1376.

84. Polozov, I. V., L. Bezrukov, K. Gawrisch, and J. Zimmerberg, 2008. Progressive ordering with decreasing temperature of the phospholipids of influenza virus. *Nat. Chem. Biol.* 4:248–255.

85. Polozov, I. V., and K. Gawrisch, 2004. Domains in binary SOPC/POPE lipid mixtures studied by pulsed field gradient 1H MAS NMR. *Biophys. J.* 87:1741–1751.

86. Ulrich, K., M. Sanders, F. Grinberg, P. Galvosas, and S. Vasenkov, 2008. Application of pulsed field gradient NMR with high gradient strength for studies of self-diffusion in lipid membranes on the nanoscale. *Langmuir* 24:7365–7370.

87. Macdonald, P. M., Q. Saleem, A. Lai, and H. H. Morales, 2013. NMR methods for measuring lateral diffusion in membranes. *Chem. Phys. Lipids* 166:31–44.

88. Tocanne, J.-F., L. Cézanne, A. Lopez, B. Piknova, V. Schram, J.-F. Tournier, and M. Welby, 1994. Lipid domains and lipid/protein interactions in biological membranes. *Chem. Phys. Lipids* 73:139–158.

89. Brown, D. A., 2001. Seeing is believing: visualization of rafts in model membranes. *Proc. Natl. Acad. Sci. U. S. A.* 98:10517–10518.

90. Šachl, R., J. Humpolíčková, M. Štefl, L. B.-Å. Johansson, and M. Hof, 2011. Limitations of electronic energy transfer in the determination of lipid nanodomain sizes. *Biophys. J.* 101:L60–L62.

91. Stillwell, W., L. J. Jenski, M. Zerouga, and A. C. Dumaual, 2000. Detection of lipid domains in docosahexaenoic acid-rich bilayers by acyl chain-specific FRET probes. *Chem. Phys. Lipids* 104:113–132.

92. Feigenson, G. W., and J. T. Buboltz, 2001. Ternary phase diagram of dipalmitoyl-PC/dilauroyl-PC/cholesterol: nanoscopic domain formation driven by cholesterol. *Biophys. J.* 80:2775–2788.

93. Toledo, A., Z. Huang, J. L. Coleman, E. London, and J. L. Benach, 2018. Lipid rafts can form in the inner and outer membranes of Borrelia burgdorferi and have different properties and associated proteins. *Mol. Microbiol.* 108:63–76.

94. Sengupta, P., D. Holowka, and B. Baird, 2007. Fluorescence resonance energy transfer between lipid probes detects nanoscopic heterogeneity in the plasma membrane of live cells. *Biophys. J.* 92:3564–3574.

95. Kreder, R., K. A. Pyrshev, Z. Darwich, O. A. Kucherak, Y. Meély, and A. S. Klymchenko, 2015. Solvatochromic Nile Red probes with FRET quencher reveal lipid order heterogeneity in living and apoptotic cells. *ACS Chem. Biol.* 10:1435–1442.

96. Silvius, J. R., and I. R. Nabi, 2006. Fluorescence-quenching and resonance energy transfer studies of lipid microdomains in model and biological membranes. *Mol. Membr. Biol.* 23:5–16.

97. Sustarsic, M., and A. N. Kapanidis, 2015. Taking the ruler to the jungle: single-molecule FRET for understanding biomolecular structure and dynamics in live cells. *Curr. Opin. Struct. Biol.* 34:52–59.

98. Chmelová, B., D. Davidoviḱ, and R. Šachl, 2022. Interleaflet organization of membrane nanodomains: What can (not) be resolved by FRET? *Biophys. J.* .

99. Enoki, T. A., F. A. Heberle, and G. W. Feigenson, 2018. FRET detects the size of nanodomains for coexisting liquid-disordered and liquid-ordered phases. *Biophys. J.* 114:1921–1935.

100. Vinklŕek, I. S., L. Vel'as, P. Riegerov;, K. Skĺa, I. Mikhalyov, N. Gretskaya, M. Hof, and R. Šachl, 2019. Experimental evidence of the existence of interleaflet coupled nanodomains: An MC-FRET study. *J. Phys. Chem. Lett.* 10:2024–2030.

101. Scott, H. L., K. B. Kennison, T. A. Enoki, M. Doktorova, J. J. Kinnun, F. A. Heberle, and J. Katsaras, 2021. Model membrane systems used to study plasma membrane lipid asymmetry. *Symmetry* 13:1356.

102. Connell, S. D., and D. A. Smith, 2006. The atomic force microscope as a tool for studying phase separation in lipid membranes. *Mol. Membr. Biol.* 23:17–28.

103. Shan, Y., and H. Wang, 2015. The structure and function of cell membranes examined by atomic force microscopy and single-molecule force spectroscopy. *Chemical Society Reviews* 44:3617–3638.

104. Dumitru, A. C., L. Conrard, C. L. Giudice, P. Henriet, M. Veiga-da Cunha, S. Derclaye, D. Tyteca, and D. Alsteens, 2018. High-resolution mapping and recognition of lipid domains using AFM with toxin-derivatized probes. *Chem. Commun.* 54:6903–6906.

105. García-Arribas, A. B., F. M. Goñi, and A. Alonso, 2021. Lipid self-assemblies under the atomic force microscope. *Int. J. Mol. Sci.* 22:10085.

106. Owen, D. M., and K. Gaus, 2013. Imaging lipid domains in cell membranes: the advent of super-resolution fluorescence microscopy. *Front. Plant Sci.* 4:503.

107. Sezgin, E., 2017. Super-resolution optical microscopy for studying membrane structure and dynamics. *J. Phys. Condens. Matter.* 29:273001.

108. Kraft, M. L., and H. A. Klitzing, 2014. Imaging lipids with secondary ion mass spectrometry. *Biochim. Biophys. Acta Mol. Cell. Biol. Lipids* 1841:1108–1119.

109. Baron, A. Q., 2020. High-resolution inelastic X-ray scattering I: Context, spectrometers, samples, and superconductors. *Cham: Springer* 2131–2212.

110. Bolmatov, D., D. Zav'yalov, M. Zhernenkov, E. T. Musaev, and Y. Q. Cai, 2015. Unified phonon-based approach to the thermodynamics of solid, liquid and gas states. *Annals of Physics* 363:221–242.

111. Bolmatov, D., E. T. Musaev, and K. Trachenko, 2013. Symmetry breaking gives rise to energy spectra of three states of matter. *Scientific Reports* 3:1–4.

112. Bolmatov, D., V. Brazhkin, and K. Trachenko, 2012. The phonon theory of liquid thermodynamics. *Scientific Reports* 2:1–6.

113. Bolmatov, D., M. Zhernenkov, D. Zav'yalov, S. N. Tkachev, A. Cunsolo, and Y. Q. Cai, 2015. The Frenkel Line: a direct experimental evidence for the new thermodynamic boundary. *Scientific Reports* 5:1–10.

114. Brockhouse, B. N., 1955. Neutron scattering and the frequency distribution of the normal modes of vanadium metal. *Canadian Journal of Physics* 33:889–891.

115. Brockhouse, B. N., 1995. Slow neutron spectroscopy and the grand atlas of the physical world. *Reviews of Modern Physics* 67:735.

116. Busch, S., C. Smuda, L. C. Pardo, and T. Unruh, 2010. Molecular mechanism of long-range diffusion in phospholipid membranes studied by quasielastic neutron scattering. *Journal of the American Chemical Society* 132:3232–3233.

117. Chen, S., C. Liao, H. Huang, T. Weiss, M. Bellisent-Funel, and F. Sette, 2001. Collective dynamics in fully hydrated phospholipid bilayers studied by inelastic X-ray scattering. *Physical Review Letters* 86:740.

118. Weiss, T. M., P.-J. Chen, H. Sinn, E. E. Alp, S.-H. Chen, and H. W. Huang, 2003. Collective chain dynamics in lipid bilayers by inelastic X-ray scattering. *Biophysical journal* 84:3767–3776.

119. Hub, J. S., T. Salditt, M. C. Rheinstädter, and B. L. De Groot, 2007. Short-range order and collective dynamics of DMPC bilayers: a comparison between molecular dynamics simulations, x-ray, and neutron scattering experiments. *Biophysical journal* 93:3156–3168.

120. Bolmatov, D., J. J. Kinnun, J. Katsaras, and M. O. Lavrentovich, 2020. Phonon-mediated lipid raft formation in biological membranes. *Chemistry and Physics of Lipids* 232:104979.

121. Zhernenkov, M., D. Bolmatov, D. Soloviov, K. Zhernenkov, B. P. Toperverg, A. Cunsolo, A. Bosak, and Y. Q. Cai, 2016. Revealing the Mechanism of Passive Transport in Lipid Bilayers via Phonon-Mediated Nanometre-Scale Density Fluctuations. *Nat. Commun.* 7:1–10.

122. Bolmatov, D., Y. Q. Cai, D. Zav'yalov, and M. Zhernenkov, 2018. Crossover from Picosecond Collective to Single Particle Dynamics Defines the Mechanism of Lateral Lipid Diffusion. *Biochimica et Biophysica Acta (BBA)-Biomembranes* 1860:2446–2455.

123. Bolmatov, D., D. Soloviov, M. Zhernenkov, D. Zav'yalov, E. Mamontov, A. Suvorov, Y. Q. Cai, and J. Katsaras, 2020. Molecular picture of the transient nature of lipid rafts. *Langmuir* 36:4887–4896.

124. Vaz, W. L., R. M. Clegg, and D. Hallmann, 1985. Translational diffusion of lipids in liquid crystalline phase phosphatidylcholine multibilayers. A comparison of experiment with theory. *Biochemistry* 24:781–786.

125. Lindblom, G., G. Orädd, and A. Filippov, 2006. Lipid lateral diffusion in bilayers with phosphatidylcholine, sphingomyelin and cholesterol: An NMR study of dynamics and lateral phase separation. *Chem. Phys. Lipids* 141:179–184.

126. Scheidt, H. A., D. Huster, and K. Gawrisch, 2005. Diffusion of cholesterol and its precursors in lipid membranes studied by 1H pulsed field gradient magic angle spinning NMR. *Biophys. J.* 89:2504–2512.

127. Bolmatov, D., M. Zhernenkov, D. Zav'yalov, S. Stoupin, Y. Q. Cai, and A. Cunsolo, 2015. Revealing the mechanism of the viscous-to-elastic crossover in liquids. *Journal of Physical Chemistry Letters* 6:3048–3053.

128. Bolmatov, D., M. Zhernenkov, D. Zav'yalov, S. Stoupin, A. Cunsolo, and Y. Q. Cai, 2016. Thermally triggered phononic gaps in liquids at THz scale. *Scientific reports* 6:1–7.

129. Bolmatov, D., Q. Zhang, D. Soloviov, Y. M. Li, J. G. Werner, A. Suvorov, Y. Q. Cai, U. Wiesner, M. Zhernenkov, and J. Katsaras, 2018. Nanoscale Q-resolved phonon dynamics in block copolymers. *ACS Applied Nano Materials* 1:4918–4926.

130. Bolmatov, D., M. Zhernenkov, D. Zav'yalov, Y. Q. Cai, and A. Cunsolo, 2016. Terasonic excitations in 2D gold nanoparticle arrays in a water matrix as revealed by atomistic simulations. *Journal of Physical Chemistry C* 120:19896–19903.

131. Bolmatov, D., M. Zhernenkov, L. Sharpnack, D. M. Agra-Kooijman, S. Kumar, A. Suvorov, R. Pindak, Y. Q. Cai, and A. Cunsolo, 2017. Emergent optical phononic modes upon nanoscale mesogenic phase transitions. *Nano Letters* 17:3870–3876.

132. Bolmatov, D., D. Soloviov, D. Zav'yalov, L. Sharpnack, D. M. Agra-Kooijman, S. Kumar, J. Zhang, M. Liu, and J. Katsaras, 2018. Anomalous nanoscale optoacoustic phonon mixing in nematic mesogens. *The Journal of Physical Chemistry Letters* 9:2546–2553.

133. Bolmatov, D., D. Zav'yalov, J.-M. Carrillo, and J. Katsaras, 2020. Fractal boundaries underpin the 2D melting of biomimetic rafts. *Biochimica et Biophysica Acta (BBA)-Biomembranes* 1862:183249.

134. Almeida, P. F., W. L. Vaz, and T. Thompson, 1992. Lateral diffusion in the liquid phases of dimyristoylphosphatidylcholine/cholesterol lipid bilayers: a free volume analysis. *Biochemistry* 31:6739–6747.

135. Egelman, E. H., 2016. The current revolution in cryo-EM. *Biophysical Journal* 110:1008–1012.

136. Milne, J. L., M. J. Borgnia, A. Bartesaghi, E. E. Tran, L. A. Earl, D. M. Schauder, J. Lengyel, J. Pierson, A. Patwardhan, and S. Subramaniam, 2013. Cryo-electron microscopy–a primer for the non-microscopist. *The FEBS journal* 280:28–45.

137. Henderson, R., and P. N. T. Unwin, 1975. Three-dimensional model of purple membrane obtained by electron microscopy. *Nature* 257:28–32.

138. Taylor, K. A., and R. M. Glaeser, 1974. Electron diffraction of frozen, hydrated protein crystals. *Science* 186:1036–1037.

139. Dubochet, J., M. Adrian, J.-J. Chang, J.-C. Homo, J. Lepault, A. W. McDowall, and P. Schultz, 1988. Cryo-electron microscopy of vitrified specimens. *Quarterly reviews of biophysics* 21:129–228.

140. Scott, H. L., A. Skinkle, E. G. Kelley, M. N. Waxham, I. Levental, and F. A. Heberle, 2019. On the mechanism of bilayer separation by extrusion, or why your LUVs are not really unilamellar. *Biophysical journal* 117:1381–1386.

141. Wang, L., P. S. Bose, and F. J. Sigworth, 2006. Using cryo-EM to measure the dipole potential of a lipid membrane. *Proceedings of the National Academy of Sciences* 103:18528–18533.

142. Tahara, Y., and Y. Fujiyoshi, 1994. A new method to measure bilayer thickness: cryo-electron microscopy of frozen hydrated liposomes and image simulation. *Micron* 25:141–149.

143. Heberle, F. A., M. Doktorova, H. L. Scott, A. D. Skinkle, M. N. Waxham, and I. Levental, 2020. Direct label-free imaging of nanodomains in biomimetic and biological membranes by cryogenic electron microscopy. *Proceedings of the National Academy of Sciences* 117:19943–19952.

144. Cornell, C. E., A. Mileant, N. Thakkar, K. K. Lee, and S. L. Keller, 2020. Direct imaging of liquid domains in membranes by cryo-electron tomography. *Proceedings of the National Academy of Sciences* 117:19713–19719.

145. Soranzo, T., D. Martin, J. Lenormand, and E. Watkins, 2017. Coupling neutron reflectivity with cell-free protein synthesis to probe membrane protein structure in supported bilayers. *Sci Rep* 7:3399.

146. Clifton, L. A., S. A. Holt, A. V. Hughes, E. L. Daulton, W. Arunmanee, F. Heinrich, S. Khalid, D. Jefferies, T. R. Charlton, J. R. P. Webster, C. J. Kinane, and J. H. Lakey, 2015. An accurate in vitro model of the E. coli envelope. *Angew. Chem.* 54(41):11952–11955.

147. Fragneto, G., 2012. Neutrons and model membranes. *Eur. Phys. J. Spec. Top.* 213:327–342.

148. Skoda, M. W., 2019. Recent developments in the application of X-ray and neutron reflectivity to soft-matter systems. *Curr. Opin. Colloid Interface Sci.* 42:41–54.

149. Majkrzak, C., and N. Berk, 1995. Exact determination of the phase in neutron reflectometry. *Phys. Rev. B* 52:10827.

150. Majkrzak, C., N. Berk, J. Dura, S. Satija, A. Karim, J. Pedulla, and R. Deslattes, 1997. Direct inversion of specular reflectometry. *Physica B Condens. Matter* 241:1101–1103.

151. Burns, A., D. Frankel, and T. Buranda, 2005. Local mobility in lipid domains of supported bilayers characterized by atomic force microscopy and fluorescence correlation spectroscopy. *Biophys. J.* 89:1081–1093.

152. Seu, K. J., A. P. Pandey, F. Haque, E. A. Proctor, A. E. Ribbe, and J. S. Hovis, 2007. Effect of surface treatment on diffusion and domain formation in supported lipid bilayers. *Biophys. J.* 92:2445–2450.

153. Kiessling, V., S.-T. Yang, and L. K. Tamm, 2015. Supported lipid bilayers as models for studying membrane domains. *Curr. Top. Membr.* 75:1–23.

154. Clifton, L. A., M. W. Skoda, E. L. Daulton, A. V. Hughes, A. P. LeBrun, J. H. Lakey, and S. A. Holt., 2013. An accurate in vitro model of the E. coli envelope. *Journal of The Royal Society Interface* 10(89):0810.

155. Wacklin, H. P., 2010. Neutron reflection from supported lipid membranes. *Curr. Opin. Colloid Interface Sci.* 15:445–454.

156. Rondelli, V., E. Del Favero, S. Motta, L. Cantù, G. Fragneto, and P. Brocca, 2013. Neutrons for rafts, rafts for neutrons. *Eur. Phys. J. E* 36:1–8.

157. Langner, M., M. Komorowska, M. Koter, and J. Gomukiewicz, 1984. Phase transitions in spherical bilayer membranes prepared of bulk erythrocyte membrane lipids. *Gen. Physiol. Biophys* 3:521–526.

158. Scott, H. L., D. Bolmatov, P. T. Podar, Z. Liu, J. J. Kinnun, B. Doughty, R. Lydic, R. L. Sacci, C. P. Collier, and J. Katsaras, 2022. Evidence for long-term potentiation in phospholipid membranes. *Proc. Nat. Acad. Sci.* 119:e2212195119.

159. McClintic, W. T., H. L. Scott, N. Moore, M. Farahat, M. Maxwell, C. D. Schuman, D. Bolmatov, F. N. Barrera, J. Katsaras, and C. P. Collier, 2022. Heterosynaptic plasticity in biomembrane memristors controlled by pH. *MRS Bulletin* 1–9.

160. Sacci, R. L., H. L. Scott, Z. Liu, D. Bolmatov, B. Doughty, J. Katsaras, and C. P. Collier, 2022. Disentangling Memristive and Memcapacitive Effects in Droplet Interface Bilayers Using Dynamic Impedance Spectroscopy. *Advanced Electronic Materials* 8:2200121.

161. Antonov, V. F., A. A. Anosov, V. P. Norik, E. A. Korepanova, and E. Y. Smirnova, 2003. Electrical capacitance of lipid bilayer membranes of hydrogenated egg lecithin at the temperature phase transition. *Eur. Biophys. J.* 32:55–59.

162. Boheim, G., W. Hanke, and H. Eibl, 1980. Lipid phase transition in planar bilayer membrane and its effect on carrier-and pore-mediated ion transport. *Proc. Natl. Acad. Sci. U. S. A.* 77:3403–3407.

163. White, S. H., 1975. Phase transitions in planar bilayer membranes. *Biophys. J.* 15:95–117.

164. Gliozzi, A., R. Rolandi, M. De Rosa, and A. Gambacorta, 1983. Monolayer black membranes from bipolar lipids of archaebacteria and their temperature-induced structural changes. *J. Membr. Biol.* 75:45–56.

165. Lee, D. E., M. G. Lew, and D. J. Woodbury, 2013. Vesicle fusion to planar membranes is enhanced by cholesterol and low temperature. *Chem. Phys. Lipids* 166:45–54.

166. Seeger, H. M., L. Aldrovandi, A. Alessandrini, and P. Facci, 2010. Changes in single K+ channel behavior induced by a lipid phase transition. *Biophysical journal* 99:3675–3683.

167. Bayley, H., B. Cronin, A. Heron, M. A. Holden, W. L. Hwang, R. Syeda, J. Thompson, and M. Wallace, 2008. Droplet interface bilayers. *Mol. Biosyst.* 4:1191–1208.

168. Taylor, G. J., and S. A. Sarles, 2015. Heating-enabled formation of droplet interface bilayers using Escherichia coli total lipid extract. *Langmuir* 31:325–337.

169. Gross, L. C., A. J. Heron, S. C. Baca, and M. I. Wallace, 2011. Determining membrane capacitance by dynamic control of droplet interface bilayer area. *Langmuir* 27:14335–14342.

170. Taylor, G. J., G. A. Venkatesan, C. P. Collier, and S. A. Sarles, 2015. Direct in situ measurement of specific capacitance, monolayer tension, and bilayer tension in a droplet interface bilayer. *Soft matter* 11:7592–7605.

171. Taylor, G. J., F. A. Heberle, J. S. Seinfeld, J. Katsaras, C. P. Collier, and S. A. Sarles, 2017. Capacitive detection of low-enthalpy, higher-order phase transitions in synthetic and natural composition lipid membranes. *Langmuir* 33:10016–10026.

172. Heimburg, T., 2010. Lipid ion channels. *Biophys. Chem.* 150:2–22.

173. Blicher, A., K. Wodzinska, M. Fidorra, M. Winterhalter, and T. Heimburg, 2009. The temperature dependence of lipid membrane permeability, its quantized nature, and the influence of anesthetics. *Biophys. J.* 96:4581–4591.

174. Antonov, V., V. Petrov, A. Molnar, D. Predvoditelev, and A. Ivanov, 1980. The appearance of single-ion channels in unmodified lipid bilayer membranes at the phase transition temperature. *Nature* 283:585–586.

175. Marquardt, D., F. A. Heberle, T. Miti, B. Eicher, E. London, J. Katsaras, and G. Pabst, 2017. 1H NMR shows slow phospholipid flip-flop in gel and fluid bilayers. *Langmuir* 33:3731–3741.